Exploring the hydrodynamics of dense beds of Geldart B and D gas-fluidized particles through the analysis of capacitance probe signals

Laura Molignano, Maurizio Troiano, Roberto Solimene, Sina Tebianian, Jean-François Joly, Piero Salatino

Powder Technology 447 (2024) 120174

Contents lists available at ScienceDirect

Powder Technology

journal homepage: www.journals.elsevier.com/powder-technology

Exploring the hydrodynamics of dense beds of Geldart B and D gas-fluidized particles through the analysis of capacitance probe signals

Laura Molignano [a,b], Maurizio Troiano [a,c], Roberto Solimene [c,*], Sina Tebianian [b], Jean-François Joly [b], Piero Salatino [a]

[a] Dipartimento di Ingegneria Chimica, dei Materiali e della Produzione Industriale, Università degli Studi di Napoli Federico II, Piazzale Tecchio 80, 80125 Napoli, Italy
[b] Direction Conception Modélisation Procédés, IFP Energies Nouvelles, Rond-point de l'échangeur de Solaize, 69360 Solaize, France
[c] Istituto di Scienze e Tecnologie per l'Energia e la Mobilità Sostenibili, Consiglio Nazionale delle Ricerche, Piazzale Tecchio 80, 80125 Napoli, Italy

HIGHLIGHTS

- Emulsion-phase expansion is mainly associated with bubble-induced shear flow.
- Particles surface properties impact on emulsion-phase dilatancy and espansion.
- Characteristic normalized values of emulsion-phase voidages are obtained.
- The Richardson-Zaki correlation can be used for emulsion phase expansion.
- Hydrodynamics of fluidized bed dense phase impact on transport phenomena.

GRAPHICAL ABSTRACT

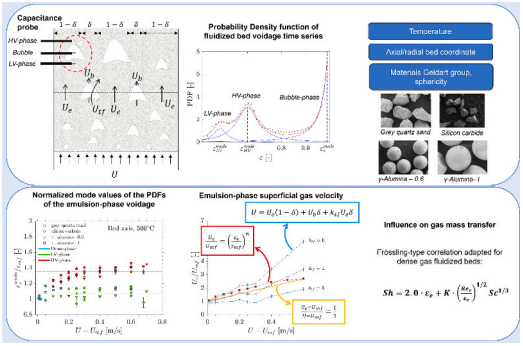

ARTICLE INFO

Keywords:
Granular solid
Bubbling fluidized bed
Emulsion-phase voidage
Gas distribution
Mass transfer
Capacitance probe

ABSTRACT

The hydrodynamics of Geldart B and D solids dense fluidized beds, of spherical/irregular morphology, have been characterized using capacitance probes at ambient temperature and 500 °C. A statistical approach applied to the time series of local bed voidage reveals, at specific experimental conditions, a characteristic bimodal distribution in the emulsion phase voidage: a more expanded, high-voidage, phase can be distinguished from a low-voidage phase with values close to minimum fluidization condition. Quantitative and qualitative differences among tested materials can be associated to different particles morphology. Emulsion phase voidages for the tested samples collapse on the same characteristic value once normalized with the voidages at incipient fluidization condition. The Richardson-Zaki equation proves to effectively correlate also in the bubbling fluidization regime the voidage and gas superficial velocity in the emulsion phase. The influence of hydrodynamics of fluidized bed dense phase on mass transfer in the emulsion phase is clearly highlighted.

* Corresponding author.
E-mail address: roberto.solimene@stems.cnr.it (R. Solimene).

https://doi.org/10.1016/j.powtec.2024.120174
Received 25 September 2023; Received in revised form 9 August 2024; Accepted 10 August 2024
Available online 12 August 2024

Notation

A	area [m^2]
d	diameter [m]
$\widetilde{d}$	mean diameter [m]
D	column diameter [m]
h	distance from distributor [m]
H	height [m]
K	fitting parameter in Frössling-type correlation [−]
k_{tf}	throughflow coefficient [−]
n	parameter in Richardson-Zaki correlation [−]
r	radius [m]
R	column radius [m]
S	column cross section [m^2]
U	superficial gas velocity [m/s]
Y	correction factor for the visible bubble flow with respect to the two-phase theory [−]

Greek symbols

δ	volume fraction of bubble phase [−]
ε	voidage [−]
$\langle\varepsilon\rangle$	spatially averaged voidage [−]
θ	polar coordinate of the bubble
κ	relative dielectric constant [−]
ρ	density [kg/m^3]
ϕ	particle sphericity [−]
σ	local LV-phase fraction in the emulsion phase [−]

Dimensionless numbers

Ar	Archimedes number [−]
Re	Reynolds number [−]
Sh	Sherwood number [−]
Sc	Schmidt number [−]

Subscripts

b	bubble
e	emulsion/dense phase
f	fluidized bed
LV	low-voidage phase
HV	high-voidage phase
i	subsection number
mf	minimum fluidization conditions
p	particle
$pack$	packed
r	radial
s	solid
t	terminal
tf	throughflow
th	threshold

Superscripts

$mode$	mode

1. Introduction

Gas fluidized bed systems are often chosen for industrial processes in which the intimate contact between the solid and gas phase is required [1]. Thus, the correct modeling of gas flow distribution is essential to the proper units design and operation. The *two-phase theory of fluidization* postulated by Toomey and Johnstone [2] has been of fundamental importance as a conceptual framework of *aggregative* fluidization for freely bubbling fluidized beds of Geldart B and D particles. Nevertheless, it is long established that, in several cases, the two-phase theory seriously overestimates the visible bubble flow [3]. Some studies attributed this discrepancy in visible bubble flow to an increase in the interstitial gas velocity in the dense phase above that required for incipient fluidization [4–6]. Further studies confirmed that the dense-phase does not remain at minimum fluidization conditions as superficial gas velocity is increased [7,8]. However, a thorough mechanistic model of the dense phase expansion for the different particle groups of Geldart classification has not been proposed so far. Other theories related the discrepancy in visible bubble flow mostly to throughflow inside bubbles [9], leading to the so-called *modified two-phase theory* [10]. Grace and Clift [3] considered this theory still oversimplified. In a more comprehensive view, Valenzuela and Glicksman [11] considered that the gas may cross the horizontal section of a conventional bubbling fluidized bed following all the mentioned mechanisms:

- as bubble voids, contributing to the visible bubble flow,
- as flow through the bubbles, known as throughflow component,
- as interstitial flow through the particles in the dense phase (not necessarily at minimum fluidization conditions).

This can be translated in the following gas balance on superficial gas velocity, U:

$$\boldsymbol{U = U_e(1-\delta) + U_b\delta + U_{tf}\delta} \tag{1}$$

where δ is the volume fraction of the bed occupied by bubbles, U_e represents the superficial gas velocity in the dense phase, U_b the bubble velocity, U_{tf} the velocity of gas passing through the bubble boundaries. All these quantities represent values averaged both in time and space. For Darcy-type gas flow in the dense phase, the gas pressure field depends only on volume, shape and location of bubbles [12] and the velocity in dense phase U_e is directly proportional to its gas permeability [11], under the assumptions of uniform value of voidage of the dense phase, ε_e, of constant volume of bubbles i.e. a net zero gas flow around the bubble boundary and of incompressible gas phase. Thus, being the bubble throughflow velocity, U_{tf} dependent only on the gas pressure field in the bubbling fluidized bed and on dense phase permeability, the interrelation between U_{tf} and U_e can be simply expressed through a proportionality coefficient, k_{tf}, resulting in:

$$\boldsymbol{U = U_e(1-\delta) + U_b\delta + k_{tf}U_e\delta} \tag{2}$$

According to Davidson's model [13], for a single three-dimensional spherical bubble in an infinite bed at the incipient fluidization condition, k_{tf} is 3, with $U_{tf} = k_{tf}U_{mf}$. Instead, Murray's analysis [14] referred to a three-dimensional spherical bubble predicts that the relative velocity between the fluid and bubble is $U_{mf}(1 + cos\theta)$, θ being the polar coordinate of the bubble. It results that the average value for k_{tf} is 1. Deviations from reported values of k_{tf} can occur for bubbles having a shape different than the spherical one, in freely bubbling fluidized bed conditions and following specific bubbles patterns [11].

Glicksman and McAndrews [15] measured the throughflow coefficient for several bed widths, but considered the dense phase at incipient fluidization conditions, even for fluidization numbers much higher than one. Olowson and Almstedt [16] measured the gas throughflow velocity inside bubbles of a 3D cold large-fluidized bed at different pressure conditions. Other researchers [17,18] performed measurements in 2D fluidized beds of isolated bubbles operated at superficial velocity slightly higher than incipient fluidization conditions. Lim et al. [19] measured a throughflow factor in a 2D fluidized bed of Geldart B solids using a gas balance where bubble, wake and dense phases were included, with the dense phase considered at minimum fluidization conditions. Wu et al. [20] run experiments in which single bubbles were injected into an incipiently 3D fluidized bed. By modifying the Sit and Grace model [21], they identified a range of throughflow coefficients,

which varied according to the operating temperature and the adopted material. Solimene et al. [22] measured local throughflow coefficients of isolated bubbles in experiments on 3D hot gas-fluidized beds of Geldart B and D solids operated at incipient fluidization conditions. Almendros-Ibáñez et al. [23] studied the effect of voidage distribution around endogenous bubbles on the throughflow component in 2D fluidized beds. Bakshi et al. [24] adopted computational fluid dynamics (CFD) to simulate bubbling fluidized beds representative of large scale units. The authors statistically determined the gas-flow distribution in fluidized beds of three distinct Geldart B particles at several superficial gas velocities. A throughflow factor, indicating the tendency for throughflow, was defined. Villanueva-Chávez and Bizzo [25] developed a one-dimensional mathematical model of the fluid dynamics and the biomass combustion process in a bubbling fluidized bed. They included the throughflow component in the gas balance and, unlike in the classic approach, the emulsion phase was considered not to remain under minimum fluidization conditions. Results were validated with experimental and CFD studies from other authors [26,27].

The coefficient k_{tf} could be deduced from the gas balance expressed in Eq. 2, if all the other terms are known. Among them, U_e is of relevance as it could be significantly different from U_{mf} and, in turn affect the term associated to the throughflow. This would have consequences on the modeling of processes in which bed hydrodynamics play a crucial role on the overall gas-solid reaction conversion [28–33].

In aggregative fluidization of Geldart B and D solids, U_e can be calculated from the relationship of Hilligardt and Werther [34], valid for three-dimensional beds:

$$\frac{U_e - U_{mf}}{U - U_{mf}} = \frac{1}{3} \tag{3}$$

Eq. 3 can be a powerful tool to predict the superficial velocity of gas percolating through the expanded emulsion-phase of a bubbling fluidized bed, despite not accounting for differences between Geldart B and D solids and possible local differences inside the dense bed.

In homogeneous fluidization, a consolidated relationship links $U_e(\equiv U)$ with $\varepsilon_e(\equiv \varepsilon_f)$:

$$\frac{U_e}{U_{mf}} = \left(\frac{\varepsilon_e}{\varepsilon_{mf}}\right)^n \tag{4}$$

Eq. 4 derives from the original form of the Richardson-Zaki correlation [35]:

$$\frac{d\,logU}{d\,log\varepsilon} = n = constant \tag{5}$$

integrated with the boundary condition: $U = U_{mf}$ at $\varepsilon = \varepsilon_{mf}$. The parameter n correlates with the Archimedes or equivalent Galileo number through the equation proposed by Khan and Richardson [36]. Eq. 5 originates from liquid fluidization. As resumed by Di Felice, several authors have confirmed its applicability to the homogeneous expansion range of gas-solid beds [37,38]. In particular, the derivation of Eqs. 4 and 5 can be analytically obtained from gas pressure loss due to particle drag and unrecoverable bed pressure loss due to the fluidization condition [39]. The idea of extending the relationship to liquid fluidized beds encountering the appearance of bubbles has been mentioned in the review of Di Felice [37]. It was also suggested that hydrodynamic modeling of bubbling fluidized beds would greatly benefit from basic input derived by liquid-solid systems studies. Indeed, long before Avidan and Yerusalemi [40] studied the applicability of the Richardson-Zaki equation to Geldart A solids fluidized in the slugging and turbulent regimes. Afterwards, Olowson and Almstedt [41] adopted the Richardson-Zaki correlation to solids at the boundary between groups B and D, fluidized in the bubbling regime, to calculate the dense-phase expansion from U_e measurements.

To better understand the actual fluidization patterns, in a recent study, Molignano et al. [42] used custom-made capacitance probes to comprehensively characterize voidage distribution in bubbling fluidized beds of grey quartz sand belonging to the group B of Geldart's classification, both at room temperature and 500 °C. Capacitance probes have been chosen due to their favourable features in terms of ease of operation and signal interpretation, temporal resolution, cost, applicability in high temperature environments and in industrial units. The signals obtained from the measurements with capacitance probes have been elaborated using a statistical approach applied to a detailed time-resolved analysis. Statistical analysis of the time-series of local bed voidage obtained at different excess gas velocities with respect to the minimum fluidization conditions revealed multimodal Probability Density Functions (PDF). A remarkable bimodal character was apparent in the portion of the spectrum that refers to the emulsion phase of the bed, more pronounced as the gas superficial velocity was increased. It has been inferred that different phases at distinctively different voidage co-exist in the emulsion phase: a lower voidage LV-phase and a higher voidage HV-phase. In the same study, a dedicated campaign consisting of fluidized bed catalytic oxidation of CO has been focused on the assessment of the mass transfer coefficient between the bulk of the bed and active particles, under the assumption of infinitely fast chemical kinetics. The outcomes of the experiment were fully consistent with the experimental findings obtained from the hydrodynamic characterization of the bed at comparable temperature. Results confirmed the close relationship between mass transfer and expansion patterns of the emulsion phase, and the need for proper hydrodynamic characterization of the bed. A more accurate version of the Frössling-type Eq. [43], modified for the estimation of mass transfer in dense fluidized beds, was proposed:

$$Sh = 2.0 \bullet \varepsilon_e + K \bullet \left(\frac{Re_e}{\varepsilon_e}\right)^{1/2} Sc^{1/3} \tag{6}$$

in which ε_e and U_e are the effective voidage and gas velocity of the emulsion phase, respectively. The modified Frössling-type correlation proposed as Eq. 6 is similar to that reported in the study of La Nauze and Jung [44], although they considered the superficial gas velocity U instead of U_e in the Reynolds number.

In the present study, the same experimental approach of Molignano et al. [42] has been used to carry out a thorough hydrodynamic characterization of different Geldart B and D solids in dense gas fluidized beds operated at room temperature and at 500 °C. Bed voidage distribution and superficial gas velocity of the emulsion phase have been obtained for each bed material, while varying the excess gas velocity with respect to minimum fluidization conditions, radial and axial coordinate of the capacitance probes. The validity of the Richardson-Zaki correlation (Eq. 4), applied to the emulsion phase of the bubbling fluidized beds, has been also investigated for the calculation of U_e and subsequent comparison with values obtained from Eq. 3 and from the gas balance of Eq. 2, in which all the main variables have been experimentally measured [16,45–49]. Main fluidization features, for instance voidage, visible bubble flow, emulsion phase velocity, obtained for the different bed materials have been compared to assess whether relevant common or different hydrodynamic patterns could be individuated.

2. Experimental

2.1. Apparatus

The apparatus used for the experiments of hydrodynamic characterization of the dense fluidized bed is based on a stainless steel 3″ diameter (schedule 40: ID 77.92 mm) and 1300 mm high column operated as atmospheric bubbling fluidized bed (Fig. 1). The fluidization gas distributor belongs to the low pressure drop type. It is a 2 mm triangular pitch perforated plate placed under two stainless steel nets (mesh size of 40 μm), which provide the major contribution to the distributor pressure drop. The average pressure drop across the gas

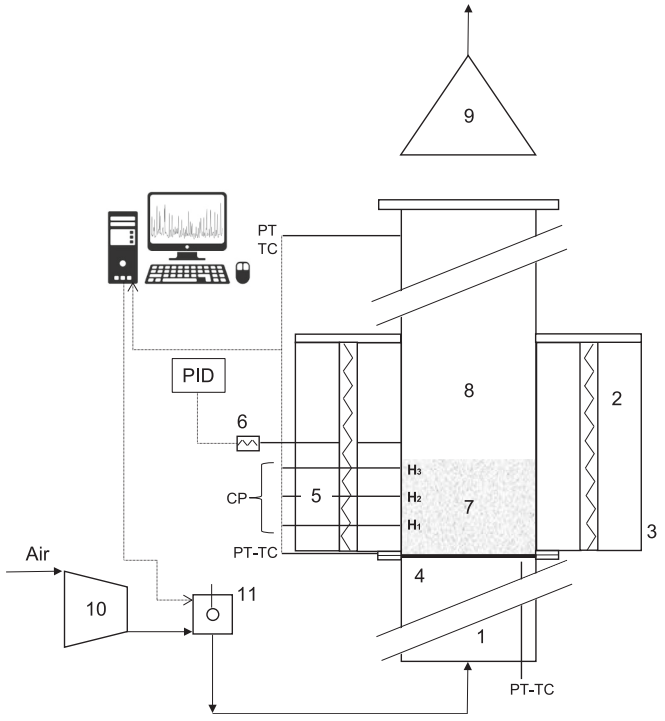

Fig. 1. Experimental apparatus for bed voidage measurement experiments. (1) Windbox; (2) electrical furnaces; (3) ceramic insulation; (4) gas distributor; (5) column lateral tubes for capacitance probes (CP); (6) thermocouple for oven PID controller; (7) bed solids; (8) fluidization column; (9) hood; (10) compressor; (11) air flowmeter. H_1=0.06 m, H_2=0.1 m, H_3=0.14 m represent the axial location of the capacitance probes in terms of distance from the distributor. PT: piezoresistive pressure transducer (operating range: 0–75 mbar); TC: K-type thermocouple.

distributor is about 173 Pa, and its ratio to the bed pressure drop ranges between 8 and 11%, depending on gas superficial velocity. These data refer to a bed inventory of 900 g and a superficial gas velocity range of 0.17–0.80 m/s at 500 °C. In Fig. 2, the down fluidization curve of one of the tested materials (grey quartz) is showed to demonstrate that proper fluidization conditions were assured. The windbox is a 225 mm high stainless steel column filled with ceramic rings to equalize the gas flow. The fluidization column is thermally insulated and heated by two semi-

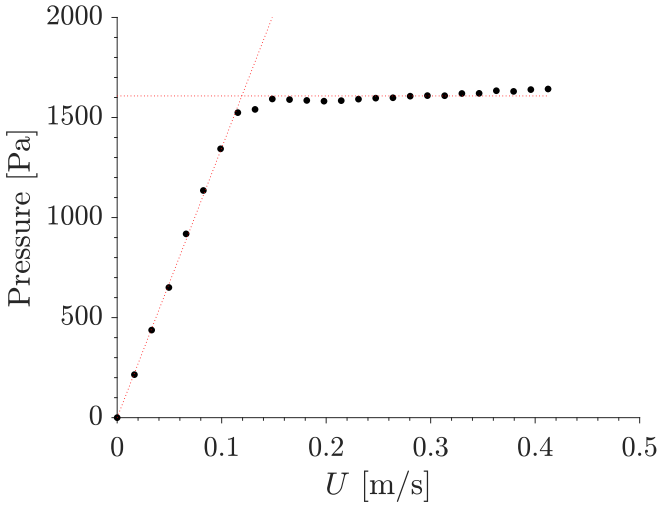

Fig. 2. Fluidization curve of grey quartz sand ($\widetilde{d}_p = 505$ μm, $\rho_p = 2650$ kg/m^3) obtained by progressively decreasing the superficial gas velocity at 500 °C in the experimental apparatus showed in Fig. 1.

cylindrical 2.4 kW ceramic ovens, while the bed temperature is kept at the set point by a PID control unit. Gases are fed to the column via high-precision digital mass flowmeters/controllers. Entrained dust, which results from the abrasion of dense bed particles during testing, is removed via a fume hood.

The two ports located under and right above the gas distributor, respectively, are 4 mm ID tubes exclusively used for pressure and temperature measurements. The second pressure tap is located at 0.01 m above the grid. The column presents other six 3/8″ diameter (schedule 40: ID 12.4 mm) tubes, mounted flush to the column wall, that provide access to capacitance probes and for pressure/temperature measurements. These lateral accesses are placed at different vertical positions along the column, at distances above the distributor plate of 0.06, 0.1, 0.14, 0.18, 0.34 and 0.95 m. In Fig. 1 only the ports which have been used for the experiments are represented. Each measurement probe is connected to its data acquisition module and signals are acquired simultaneously on a Personal Computer via a program developed in LabVIEW.

2.2. Materials

Four different bed solids were tested in the hydrodynamic characterization experiments: grey quartz sand, silicon carbide and two γ-alumina samples. Material properties are listed in Table 1. Grey quartz sand and silicon carbide were conditioned at 800 °C and double sieved in a relatively narrow particle size range of 420–590 μm. γ-alumina samples do not need this kind of conditioning procedure due to their spherical shape. For the first two solids, the mean diameter, $\widetilde{d}_p$, derives from the arithmetic mean between the sieving range limits of 420 and 590 μm. The γ-alumina samples are composed by mono-sized particles. ε_{mf} values at ambient temperature were considered equal to the loose bed voidages [50]. The loose bed voidage, as well as the packed bed voidage, ε_{pack}, was measured in a graduated cylinder of 500 ml so that wall effects could be minimized [51]. ε_{mf} at 500 °C for the four samples was calculated from Ergun equation [52] starting from the actual

Table 1
Properties of bed materials.

Material	Grey quartz sand	Silicon carbide	γ-Alumina–0.6	γ-Alumina–1
Sieving range, d_p [μm]	420–590	420–590	Monosize	Monosize
$\widetilde{d}_p$ [μm]	505	505	610	1000
ϕ [−]	0.64	0.63	1	1
ρ_p [kg/m^3]	2650	3253	1187	1209
ρ_{pack}(20° C) [kg/m^3]	1488	1764	774	779
Geldart group	B	B/D	B	D
U_{mf}(20° C) [m/s] (experimental)	0.207	0.305	0.191	0.411
U_{mf}(500° C) [m/s] (experimental)	0.119	0.190	0.106	0.300
U_t(20° C) [m/s] (Haider and Levenspiel, 1989) [52]	2.44	2.72	3.14	4.72
U_t(500° C) [m/s] (Haider and Levenspiel, 1989) [52]	3.13	3.58	3.28	5.97
ε_{pack}(20° C) [−]	0.44	0.46	0.35	0.33
ε_{mf}(20° C) [−]	0.48	0.5	0.39	0.43
ε_{mf}(500° C) [−] (Ergun, 1952) [52]	0.49	0.52	0.43	0.43
κ_s(20° C) [−] (experimental)	3.5	12.7	3.0	3.3
κ_s(500° C) [−] (experimental)	6.2	11.8	2.6	2.7

particles diameter, density and sphericity, the experimental U_{mf} and gas properties at 500 °C. This procedure, suggested by Knowlton [53], has been adopted by Formisani et al. [54]. The sphericity of grey quartz sand and silicon carbide, ϕ, was obtained as an adjustable parameter from Ergun equation starting from solids and gas properties at ambient temperature. ϕ values seem to be reasonable in either case, as demonstrated by SEM images (Fig. 3) of the samples. The classification into Geldart groups [52] has been accomplished considering the emulsion phase interstitial gas velocity referred to minimum fluidization conditions compared to the mean bubble velocity, measured at each investigated experimental condition from the analysis of time-resolved signals of the capacitance probes. Grey quartz sand and γ-alumina–0.6 exhibit mean bubble velocity which exceeds the interstitial gas velocity of the emulsion phase at minimum fluidization conditions both at room temperature and 500 °C (fast bubbles). Thus, they certainly belong to B group particles. Silicon carbide bed shows an intermediate behavior: it presents slow bubbles at ambient temperature, but fast bubbles at 500 °C. γ-Alumina–1 is undoubtedly a type-D material (slow bubbles).

2.3. Diagnostics and experimental procedure

House-made needle-type uncooled capacitance probes have been used as main diagnostics for the hydrodynamic characterization of the dense fluidized bed of each described material in the bubbling regime. The probe needle outer diameter of 1.6 mm minimizes footprint effects. A detailed description of the probes design, their operating principle and main equations is provided in Molignano et al. [42].

The four materials have been fluidized with air at ambient temperature and at 500 °C. The same excess gas superficial velocities with respect to incipient fluidization, in the range of 0.01–0.35 m/s, were applied for the two investigated temperatures and for each bed material. Additional excess gas velocities were tested at 500 °C, up to 0.7 m/s.

The adopted experimental conditions refer to fluidized beds operated in the bubbling regime. This has been verified from the analysis of bed pressure signals both in the time and frequency domain. In Fig. 4A, the Power Spectral Density (PSD) of a pressure signal measured in the bed of grey quartz sand fluidized at 500 °C and an excess superficial gas velocity with respect to minimum fluidization conditions of 0.6 m/s is shown as an example. The characteristic frequencies of bed pressure signals recorded at the highest superficial gas velocities range from about 2 to 4 for the four samples at the two investigated temperatures. These values of dominant frequency confirm the absence of slugging regime that would present lower characteristic frequencies around 0.8, according to the relationship reported by Falkowsky and Brown [55].

In Fig. 4B, the standard deviations of absolute pressure signals measured in the bed of grey quartz sand fluidized at 500 °C are represented as an example. The standard deviation of absolute pressure fluctuations, measured at different bed heights, has also been computed for all the adopted experimental conditions, revealing that the transition to turbulent fluidization is never reached in any experimental condition investigated [56]. Therefore, each bed material was fluidized in a rather vigorous bubbling regime at the maximum investigated value of superficial gas velocity.

The amount of bed material loaded in the column was such that the packed bed aspect ratio, H/D, was in the range 1.6–1.7 for the four samples. The capacitance signal was recorded at three different axial positions inside the bed, H_1, H_2 and H_3, at a distance from the distributor plate of 0.06 and 0.1 and 0.14 m (Fig. 1). At each bed height, capacitance probes were placed at three radial positions, namely bed center, mid-radius and wall, corresponding to r/R ratios of 0, 1/2 and 7/9, respectively. For each run, capacitance signals were acquired using LabVIEW software for 180 s with a sampling frequency of 1 kHz. Pressure signals were also acquired simultaneously to check fluidization quality.

2.4. Data analysis

Time series of local bed voidage were obtained from time-resolved voltage-type signals of the capacitance probes. The measurement instrument equation was adopted to convert the local time-resolved voltage information into the local time-resolved relative dielectric constant of the fluidized medium. Afterwards, time series of local bed voidage could be obtained by working out the time-resolved relative dielectric constant of the medium as linear combination of the relative permittivity of the solid, κ_s, and of air, weighted on local bed voidage, ε [42]. A statistical approach has been adopted and Probability Density Functions (PDF) of the local bed voidage, using the Matlab software, were obtained. The main features of the PDFs have been compared at different superficial gas velocities, axial/radial coordinate of capacitance probe sensing volume and temperatures for each material.

At specific experimental conditions, deconvolution has been adopted

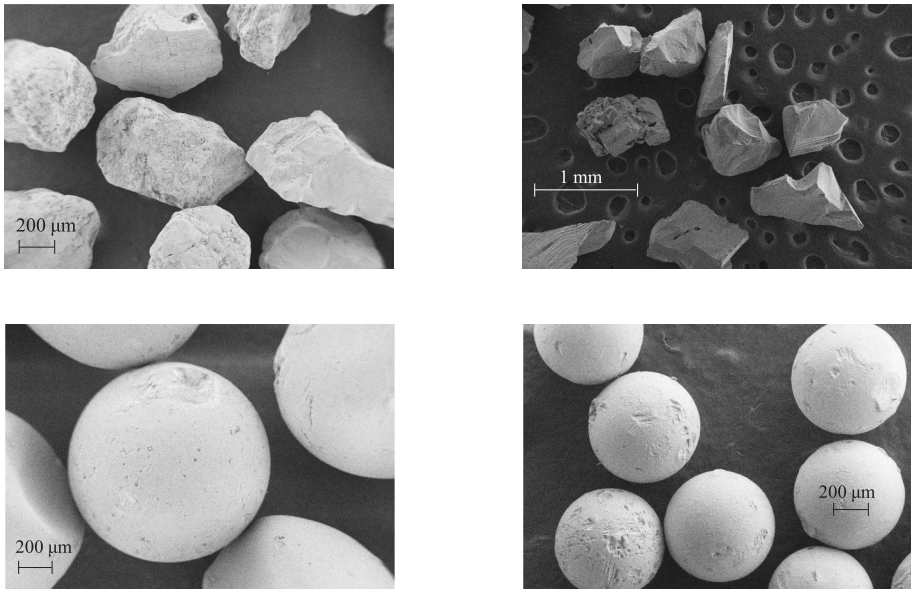

Fig. 3. SEM images of grey quartz sand and silicon carbide after conditioning, γ-alumina–1 and γ-alumina–0.6 particles (from up and left to down and right) used in the experiments.

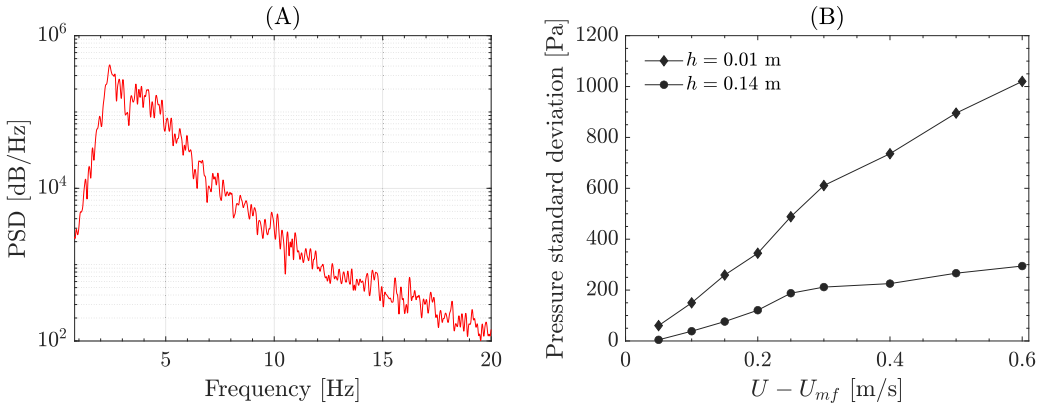

Fig. 4. (A) PSD of a pressure signal measured in the bed of grey quartz sand fluidized at 500 °C and $U - U_{mf} = 0.6$ m/s; (B) standard deviations of absolute pressure signals measured in the bed of grey quartz sand fluidized at 500 °C; h represents the distance from the gas distributor.

as it is a powerful tool in which the complex PDF of time-resolved voidage signal is decomposed into its overlapping distributions (Fig. 5). Lorentzian-type polynomials have been chosen to avoid any assumption on the shape of each monomodal distribution underlying the overall PDF. The purposely developed Matlab code is able to make multiple trial fits, taking the one to which the lowest mean fit error is associated. The number of trials was a trade-off between high accuracy and computational time. The parameter σ has been defined, in the case of a bimodal emulsion phase distribution, as the local LV-phase fraction in the emulsion phase:

$$\sigma = \frac{A_{LV}}{A_{LV} + A_{HV}} \tag{7}$$

with A_{LV} and A_{HV} representing the areas associated with the LV- and HV-distribution respectively deriving from the deconvolution procedure.

Three different methods have been chosen to calculate the superficial velocity of the gas passing through the emulsion phase, U_e, at each superficial gas velocity, U. In the first method, the equation of Hilligardt and Werther [34] has been implemented (Eq. 3). It does not require any measured quantity apart from the minimum fluidization velocity of the material at the temperature of interest. The second method involved the use of the Richardson-Zaki correlation [35] expressed according to Eq. 4. In this second case, ε_e, the characteristic voidage of the emulsion phase, is also required. The time-resolved voidage signal associated to the whole emulsion phase is extracted from the overall signal by selecting a threshold value, ε_{th}. The threshold identification at relatively high superficial gas velocities is carried out with the "method of pulses" proposed by Werther and Molerus [45]. Herein, the mean number of pulses per unit time in the time-resolved signal is obtained for different levels of voidage values (Fig. 6): the mean number of pulses per unit time rapidly increases as voidage rises from an initial value corresponding to packed conditions. After reaching a maximum, corresponding to the passage of all peaks due to porosity fluctuations in the emulsion phase and bubbles passage, the mean number of pulses per unit time decreases and the pulse count reaches a stationary value, which refers exclusively to the pulses associated to bubbles passage. Thus, the first value associated to the plateau is chosen as the threshold between the emulsion phase and the bubble phase. When the presence of bubbles is less evident, the method of pulses cannot be applied since a plateau in the plot of the mean number of pulses per unit time is not present. For such conditions, a symmetry criterion was adopted for the PDF associated to the emulsion phase, as shown in Fig. 7.

Given ε_{th}, the emulsion-phase signal was extracted from the overall signal by filtering out the parts of the signal associated to the bubbles phase. It is worth mentioning that the methodology used to obtain the emulsion phase signal, as represented in Fig. 8, excludes voidage values lower than ε_{th} that immediately precede and follow the bubble peak. The

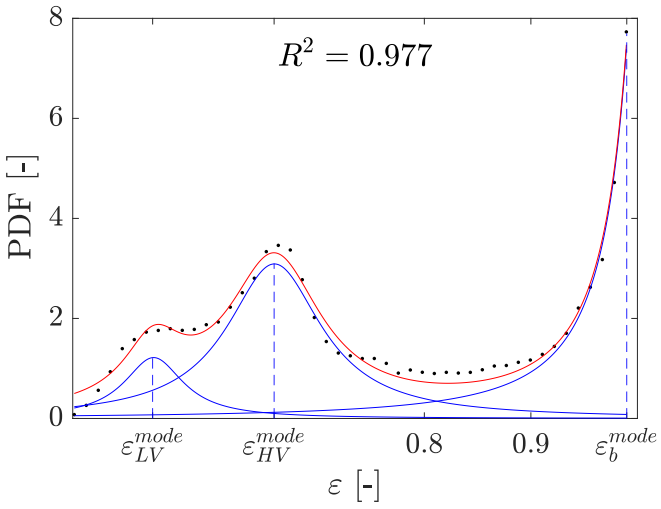

Fig. 5. Example of deconvolution of a PDF of voidage signal. Experimental conditions: fluidized bed of grey quartz sand, $T = 500$ °C, sensing volume of the probe located at bed center and H_2, $U - U_{mf} = 0.25$ m/s.

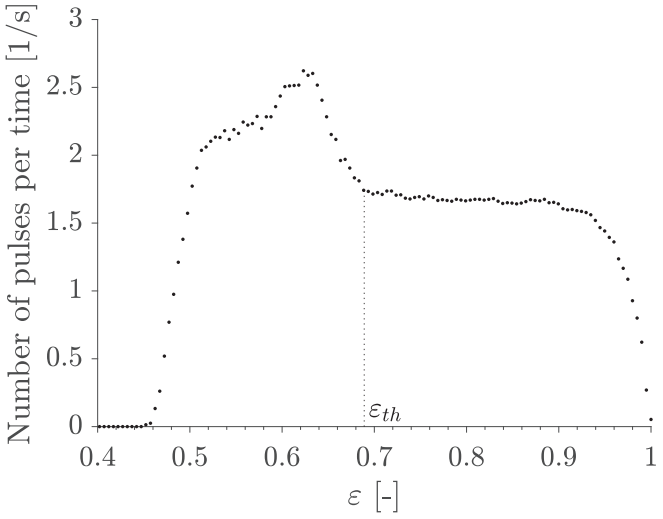

Fig. 6. Variation of the mean number of pulses per unit time in the voidage signal from grey quartz sand experiment carried out at ambient temperature and with an excess gas velocity $U - U_{mf} = 0.35$ m/s. Capacitance probe sensing volume located at H_2 and column center.

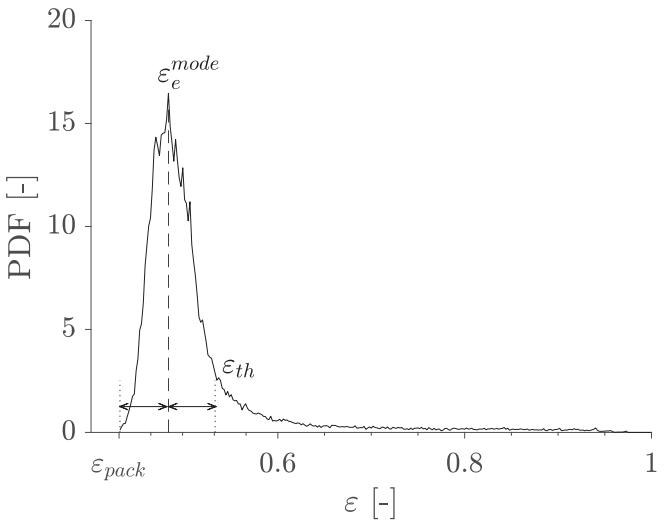

Fig. 7. Probability Density Function (PDF) of time-resolved voidage signal from grey quartz sand experiment carried out at ambient temperature and with an excess gas velocity $U - U_{mf} = 0.005$ m/s. Capacitance probe sensing volume located at H_2 and column center.

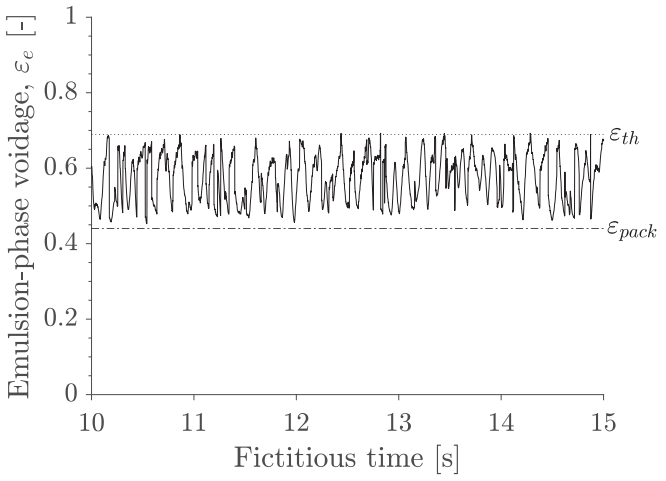

Fig. 8. Emulsion phase signal resolved over a fictitious time from grey quartz sand experiment carried out at ambient temperature and with an excess gas velocity $U - U_{mf} = 0.35$ m/s. Capacitance probe sensing volume located at H_2 and column center.

voidage signal associated to the emulsion phase was, finally, averaged over time. In Eq. 4, ε_e is the time-averaged emulsion phase voidage measured at the axial coordinate H_2 (Fig. 1), which results from the integration, over the whole cross section, of the values measured at column center, mid-radius and wall, under axisymmetric assumption.

The integration was performed by dividing the column section into three concentric subsections, S_i:

$$\langle \boldsymbol{\varepsilon} \rangle_r = \frac{\sum_{i=1}^{3} \boldsymbol{\varepsilon_e} \boldsymbol{S_i}}{\boldsymbol{S}} \tag{8}$$

with i representing the subsection number.

In the third method, a gas balance over the cross section of the fluidized bed was written according to Eq. 2. δ was derived from the mass balance on gas phase taking into account the presence of the bubble and emulsion phases:

$$\boldsymbol{\varepsilon_f} = \boldsymbol{\delta} + (\mathbf{1} - \boldsymbol{\delta})\boldsymbol{\varepsilon_e} \tag{9}$$

where the presence of small amounts of solids in bubbles was neglected. ε_f is the mean fluidized bed voidage referred to bed cross-section at the axial coordinate H_2. The mean bubble rise velocity, U_b, could be derived by adopting the cross-correlation of signals from capacitance probes sensing volumes located at H_1 and H_2 and column center. The visible bubble flow, $U_b\delta$, has been compared with values obtained using the correlation of Fu et al. [57] valid for Geldart B and D solids. As for the throughflow velocity, U_{tf}, it has been expressed as proportional to the velocity of gas passing through the emulsion phase, $k_{tf}U_e$, while considering, for the coefficient k_{tf}, values of 0 (absence of flow through bubbles), 1 [14], and 3 [13], to identify a range of possible U_{tf} values.

3. Results and discussion

3.1. Time series of fluidized bed voidage

Figs. 9–10 report selected time series of local bed voidage recorded for the four samples at 500 °C, at two different excess gas superficial velocities, with the capacitance probe sensing volume located at the column center and H_1. At the lower excess gas superficial velocity with respect to minimum fluidization conditions (Fig. 9), a signal baseline representing the emulsion-phase is recognizable, whereas upward spikes mark the passage of bubbles. It is evident that the characteristic value of the baseline signal already departs from the emulsion-phase voidage at minimum fluidization, witnessing a slight expansion of the dense-phase with respect to incipient fluidization condition. As gas superficial velocity is increased (Fig. 10) the passage of bubbles becomes more frequent, and the signal becomes more chaotic/random. In this case, it is more difficult to identify the baseline of the signal.

The general qualitative features of the voidage time series at high temperature resemble those observed at room temperature.

Time-resolved bed voidage profiles corresponding to the gas velocities, temperatures, and radial/axial locations of the capacitance probe tested for each investigated bed material indicate that:

- Local bed voidages, averaged over the entire acquisition time, ε_f, do not exhibit the same trend with temperature if results on the different materials are compared, for any given axial/radial position of the sensing volume of the probe.
- The mean local bed voidage, ε_f, is higher at the top levels H_2 and H_3 both at room and at high temperature for all the samples.
- ε_f values averaged over the radial and axial coordinate and normalized with respect to ε_{mf} result in a higher expansion of γ-alumina samples, with reference to the starting voidage condition.
- No noticeable differences arise for minimum, maximum and mean values of local bed voidage measured along the radial coordinate, for the tested materials. The transversal dimension of the fluidization column is, probably, too small to highlight significant differences along the radial coordinate.

3.2. Statistical approach for the analysis of fluidized bed voidage time series

A statistical approach on voidage time series, as already done in previous studies [8,58], has been implemented to better understand the bed hydrodynamics of the four tested materials. In the study of Molignano et al. [42], Probability Density Functions (PDF) of voidage signals, parametric in the excess gas superficial velocity with respect to minimum fluidization conditions, are reported for the grey quartz sand sample. PDFs of local voidage signals recorded during fluidization of silicon carbide, γ-alumina–1 and γ-alumina–0.6 are presented in Figs. 11–13, in which only results at 500 °C are shown for the sake of brevity. Results referred to ambient temperature conditions are reported in Figs. S.1–3 (see supplementary material). PDF curves of SiC fluidized

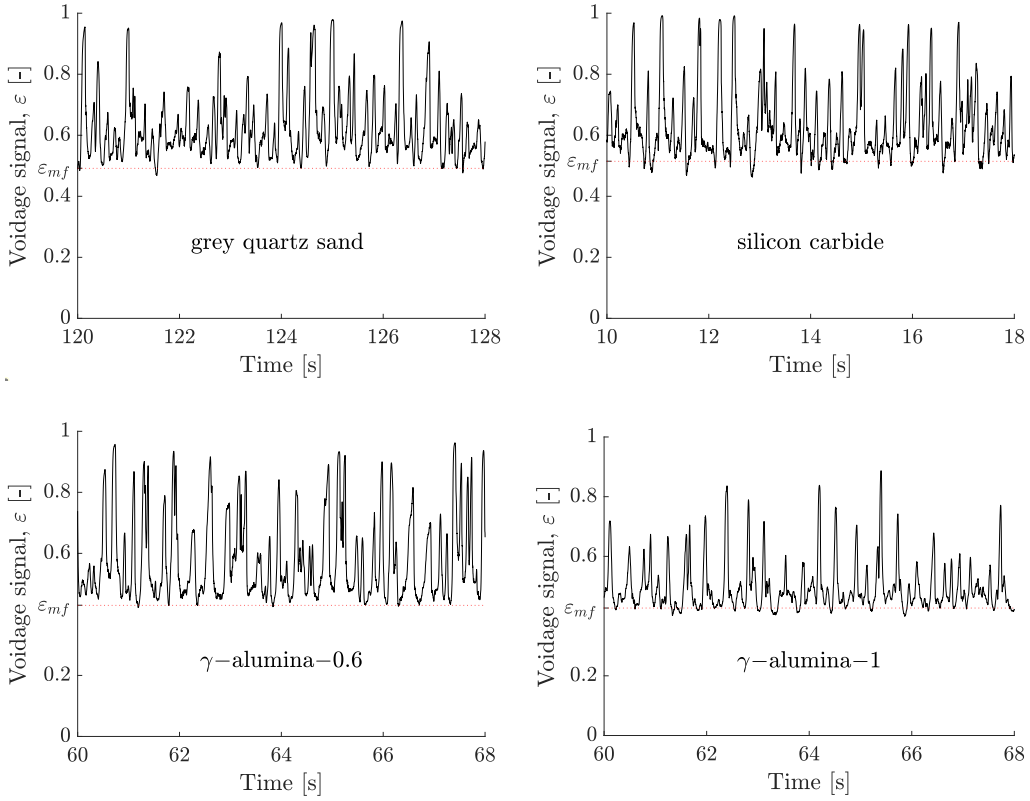

Fig. 9. Time-resolved voidage profiles. Probe radial location: center, probe level: H_1, $T = 500$ °C, $U - U_{mf} = 0.1$ m/s.

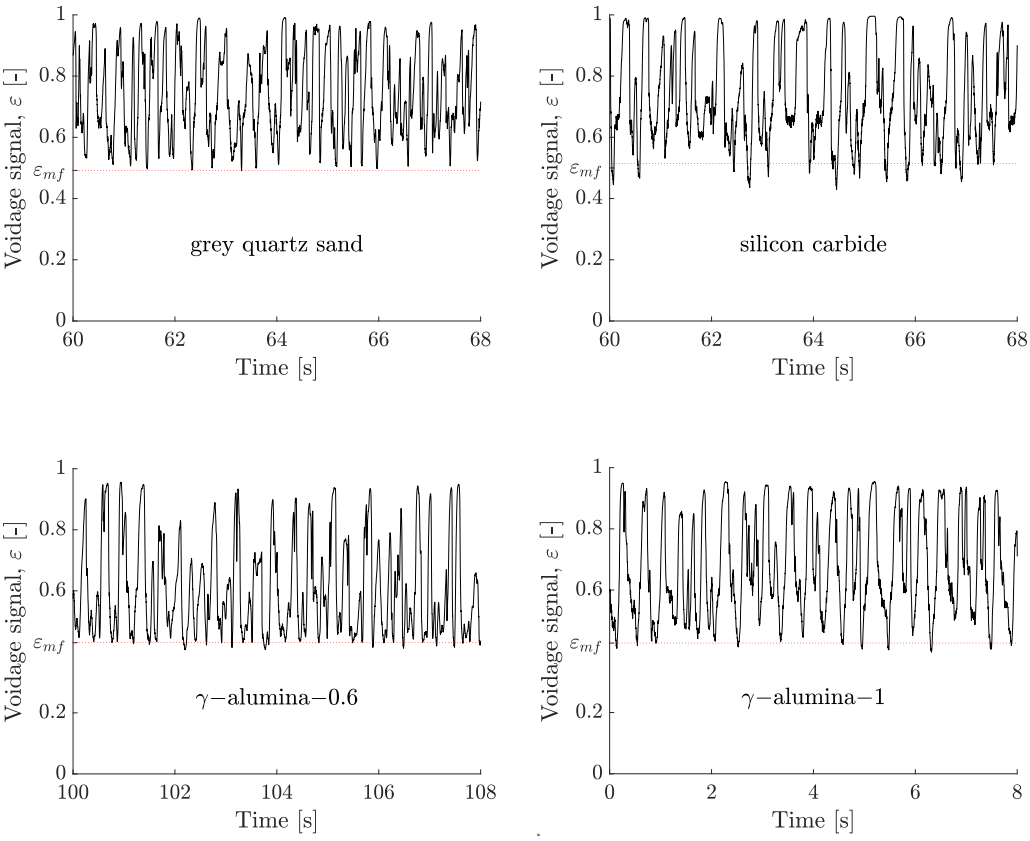

Fig. 10. Time-resolved voidage profiles. Probe radial location: center, probe level: H_1, T = 500 °C, $U - U_{mf} = 0.4$ m/s.

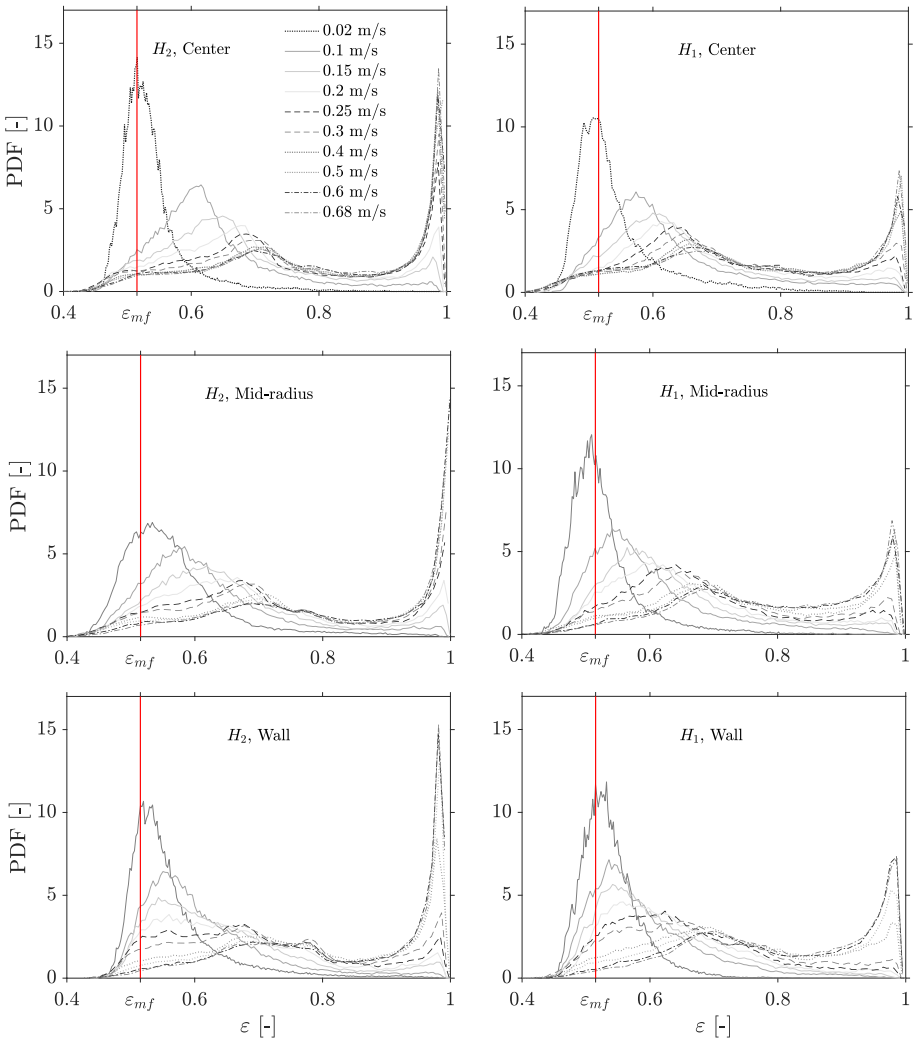

Fig. 11. Probability density functions of the local voidage of SiC fluidized bed at 500 °C for different excess gas superficial velocities and probe locations.

bed operated at 500 °C with the capacitance probe located at bed center and H_2 have been represented in separated graphs to improve the readability in Fig. S.4 (see supplementary material).

With reference to the results obtained with silicon carbide (Fig. 11), when superficial gas velocity approaches incipient fluidization conditions, the PDFs exhibit a slightly skewed unimodal trend, with a voidage modal value around ε_{mf}. Small and occasional bubbles contribute to the tail on the right-hand side of the PDF. As the gas superficial velocity is increased, a pronounced peak, representative of the bubble phase, appears at $\varepsilon \cong 1$. The bubble phase peak sharpens as $U - U_{mf}$ increases, keeping an almost constant voidage, as also observed in the study of Wytrwat et al. [49]. A zone of intermediate voidages, which separates the emulsion phase from the bubble phase, exists and exhibits a rather flat trend of low probability, if compared to those of the emulsion and bubble phases. Andreux and Chaouki [58] interpreted the same portion of the PDF obtained by bi-optical probes as being representative of the bubble cloud. In the present study, it is, instead, supposed that intermediate voidages are measured when the sensing volume of the probe is not fully covered by the dense or bubble phase. Thus, more than one phase is detected simultaneously, and an average concentration of the dense and bubble phases is measured. The extent of the area underlying the intermediate voidages zone of the PDF may probably depend on the probe sensing volume, which is, thus, an important parameter to consider for capacitance probes design. When superficial gas velocity increases, the modal value associated to the emulsion phase shifts toward higher voidages, marking the expanded state of the emulsion phase. A bimodal character in the emulsion phase becomes evident at higher superficial gas velocities and specific locations in the dense fluidized bed. The same above-listed features of silicon carbide – gathered when the probe sensing volume is placed at the axial coordinates H_1 and H_2 – have been observed in the fluidized bed of grey quartz sand [42]. The recognition of the composite, bimodal nature of the PDF component associated with the emulsion phase suggested that different phases with specific voidages co-exist in the emulsion phase: a lower voidage (LV) phase and a higher voidage (HV) phase [42]. Results on γ-alumina–1 (D group, slow or cloudless bubbles) and γ-alumina–0.6 (B group, fast or clouded bubbles) samples are reported in Figs. 12 and 13, respectively. Similarly to the cases of grey quartz sand and SiC, the PDFs exhibit a slightly skewed unimodal trend, with a voidage modal value around ε_{mf}, when superficial gas velocity approaches incipient fluidization condition. As gas superficial velocity is increased, the modal value associated to the emulsion phase shifts toward higher voidages, marking the expanded state of the emulsion-phase. As for the bimodal character of the emulsion phase, it is still present although it is less pronounced with respect to the grey quartz sand and silicon carbide. In particular, the LV- and HV-phases are more recognizable as column center and the axial coordinate H_2 are considered, whereas, in the non-mentioned cases, the bimodality is less marked or the single modal peak seems to be the merging of the two modal components. Finally, when the bimodality of the emulsion phase is more evident, the area under the portion of the

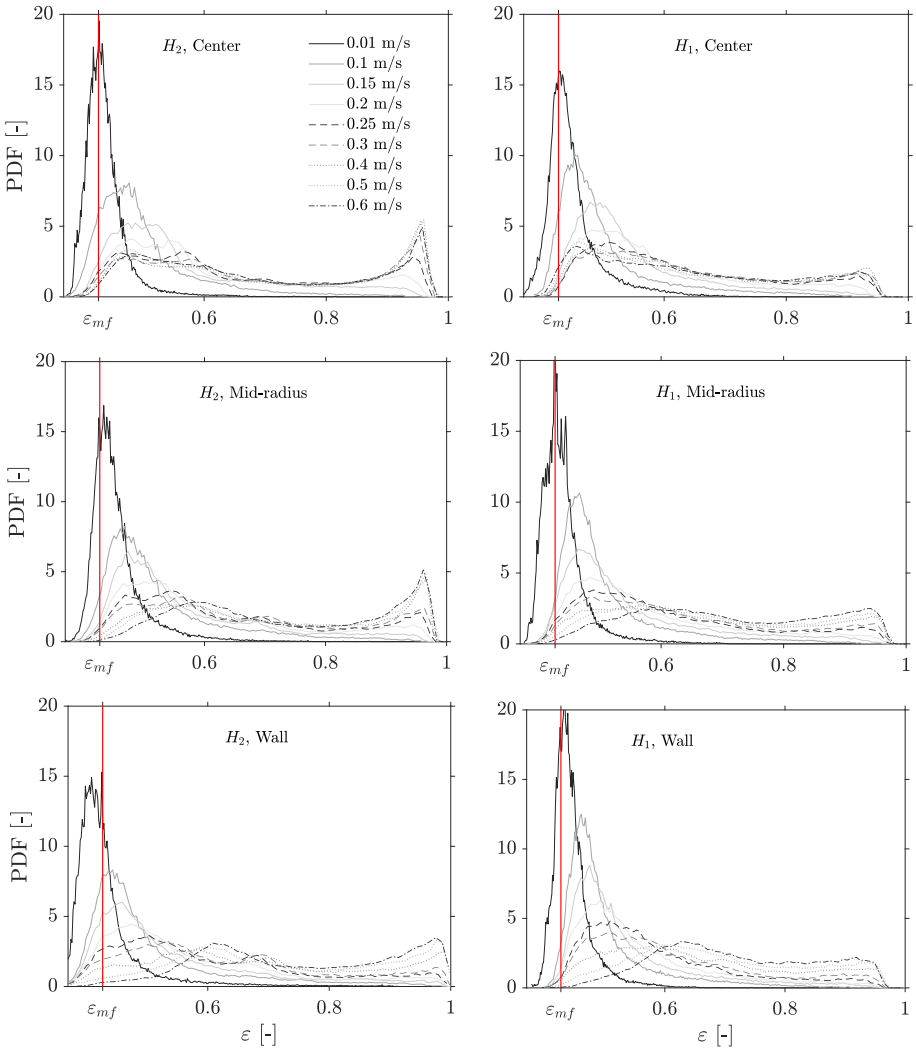

Fig. 12. Probability density functions of the local voidage of γ-alumina–1 fluidized bed at 500 °C for different excess gas superficial velocities and probe locations.

PDF curve corresponding to the LV-phase of the emulsion-phase seems to be greater in the fluidized beds of γ-alumina–1 and γ-alumina–0.6 if compared with grey quartz sand and silicon carbide samples. PDFs of time-resolved local voidage signals recorded at the axial coordinate H_3 generally do not exhibit the composite feature of the emulsion phase, but only one modal component is present, which corresponds to the expanded state of the emulsion phase. These data are reported in Figs. S.5 and 6 (see supplementary material).

The fact that bubbles might be responsible for perturbations in the dense phase has already been highlighted in literature with reference to dense-phase expansion induced by large bubbles splitting, not necessarily related to the transition from bubbling to turbulent fluidization [60]. After a detailed time-resolved analysis of voidage signals, Molignano et al. [42] speculated that the HV-phase establishes in the emulsion phase as a consequence of shear flow induced by the passage of bubbles. The broad spectrum of voidages would reflect different values of the local shear rate, that reaches a maximum as the nose of the rising bubble approaches the probe. Accordingly, expansion of the emulsion phase in the proximity of bubbles would reflect the well-established dilatancy of dense granular flows subject to shear [59]. In this framework, the LV-phase immediately trailing the bubble should correspond to solids located in the bubble wake, characterized by prevailingly coherent translational motion and scarce shear. From a completely different perspective, the localization of the HV-region on top of the bubbles [42] may drive to the conclusion that the HV-distribution is attributed to the cloud surrounding the fast bubbles of Geldart's group-B solids, which is known for being interested by high gas recirculation flow [61]. In the present study, the different investigated alumina materials belonging to both groups B (clouded bubbles) and D (cloudless bubbles) of Geldart's classification exhibited similar PDFs of local bed voidage with the presence of the HV-phase identified at some probe locations. Thus, this evidence seems to confirm the speculations of Molignano et al. [42], excluding the hypothesis that the HV-phase is related to the bubble cloud.

3.3. Major features of emulsion and bubble phase

The PDFs of the capacitance probe voidage signals for the four investigated bed materials and for each tested experimental conditions have been further analyzed to gather the major features of the emulsion phase. In particular, the peak voidages corresponding to the LV-phase and HV-phase individuated in the PDFs of voidage signal, are plotted as a function of $U - U_{mf}$ for the four bed materials in the graphs of Fig. 14. Data points are reported in a normalized form with respect to ε_{mf} of each material and for two measurement levels, H_1 and H_2. Only results at 500 °C have been shown for the sake of brevity. Results referred to ambient temperature conditions are reported in Fig. S.7 (see supplementary material). When the emulsion phase PDF preserves its monomodal shape, only one value has been plotted in light blue. This happens at relatively low superficial gas velocities for all the samples,

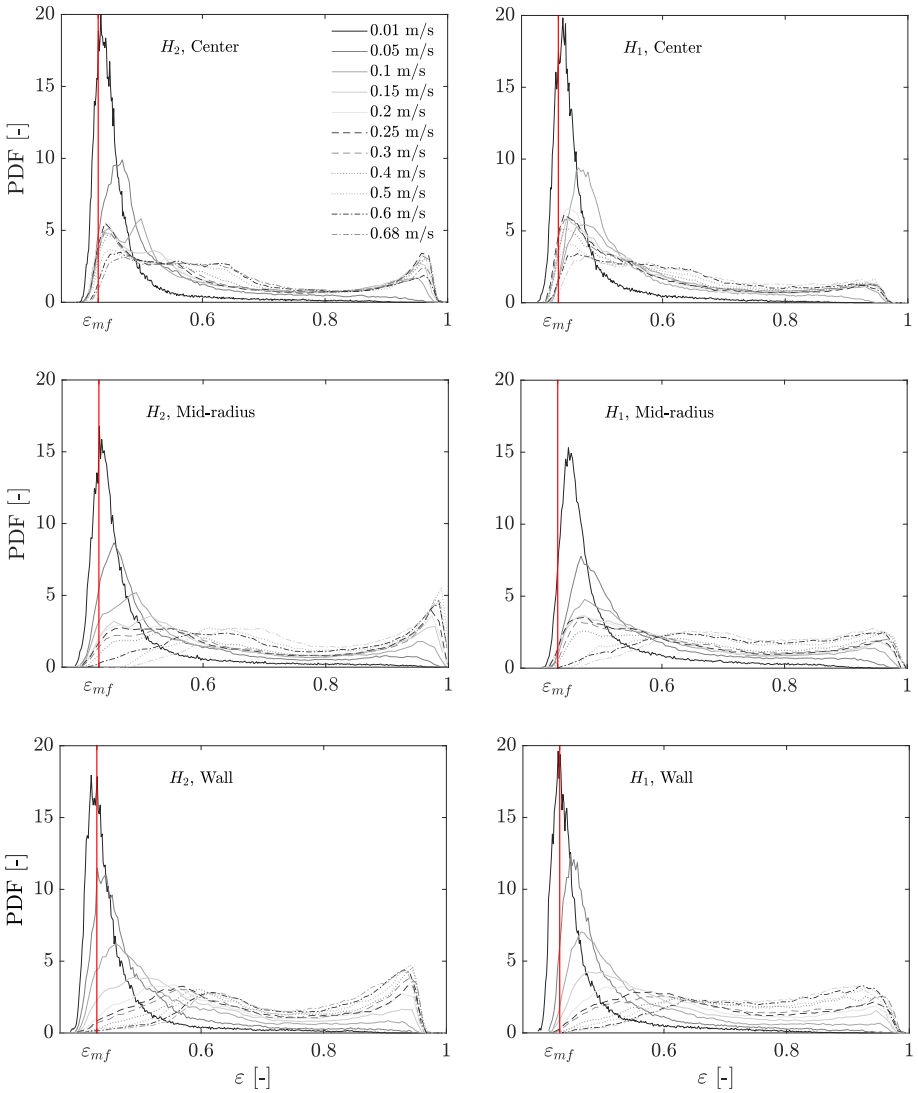

Fig. 13. Probability density functions of the local voidage of γ-alumina–0.6 fluidized bed at 500 °C for different excess gas superficial velocities and probe locations.

and also at higher superficial gas velocities with γ-alumina samples when the capacitance probe sensing volume is located at mid-radius or at the column wall. Instead, when the LV and HV phases are present and the associated peaks could be distinctively recognized from the PDFs, two data points series have been reported in green and red, respectively. In the other cases only one data points series has been shown in green or in red according to the phase peak clearly detectable. For example, when the LV distribution appears like a "shoulder" in the overall PDF, only red data points associated to the HV distribution have been reported.

It is interesting to observe that ε_e^{mode} values for the four materials tend to collapse around characteristic values when divided by the corresponding ε_{mf}. In particular, mode values of the HV-phase aggregate around values higher than unity, whereas those of the LV-phase are mostly around unity, displaying only moderate departures from ε_{mf} throughout the range of excess gas superficial velocities investigated.

Besides, the deconvolution of the PDFs into their monomodal voidage distributions was achieved at all the specific experimental conditions in which the composite nature of the emulsion phase was evident. The results of the deconvolution procedure allowed quantifying the specific weight of the LV- and HV-phases in the emulsion phase and the differences between the investigated bed materials. For instance, values of σ (ratio between the area associated with the LV-phase and the total area of the emulsion phase distribution, Eq. 7) are plotted in Fig. 15 for grey quartz and γ-alumina–1 bed materials. From the analysis of the Fig. 15, it can be observed that:

1) At ambient temperature and for the investigated interval of fluidization velocity excess the data of local fraction of the LV-phase are quite scattered and range between 0.2 and 0.4. No significant differences are observed between the two materials and a slight decreasing trend of σ with $U - U_{mf}$ is shown, even more at H_2.
2) At 500 °C for γ-alumina particles data scattering is still present in the range 0.2–0.4 similarly to data at ambient temperature. Instead, for grey quartz sand σ is less scattered and it assumes much lower values, in the range 0.05–0.2, confirming its slight decreasing trend with $U - U_{mf}$ observed at ambient temperature. In any case, no significant differences are associated with the measurement level inside the bed.

Overall, it can be concluded that the LV-phase contribution is typically smaller than that of HV-phase to the emulsion phase and it becomes less and less remarkable with irregular bed materials increasing both $U - U_{mf}$ and the bed temperature. In particular, it seems that the sphericity, ϕ, could play a key role, especially at high temperature, on the parameter σ. Indeed, it is likely that surface irregularities as well as the non-spherical particle shape (see grey quartz sand in Table 1) can emphasize the dense phase dilatancy deriving from bubble-induced shear flow [59] and, in turn, the role of HV-phase in the emulsion phase.

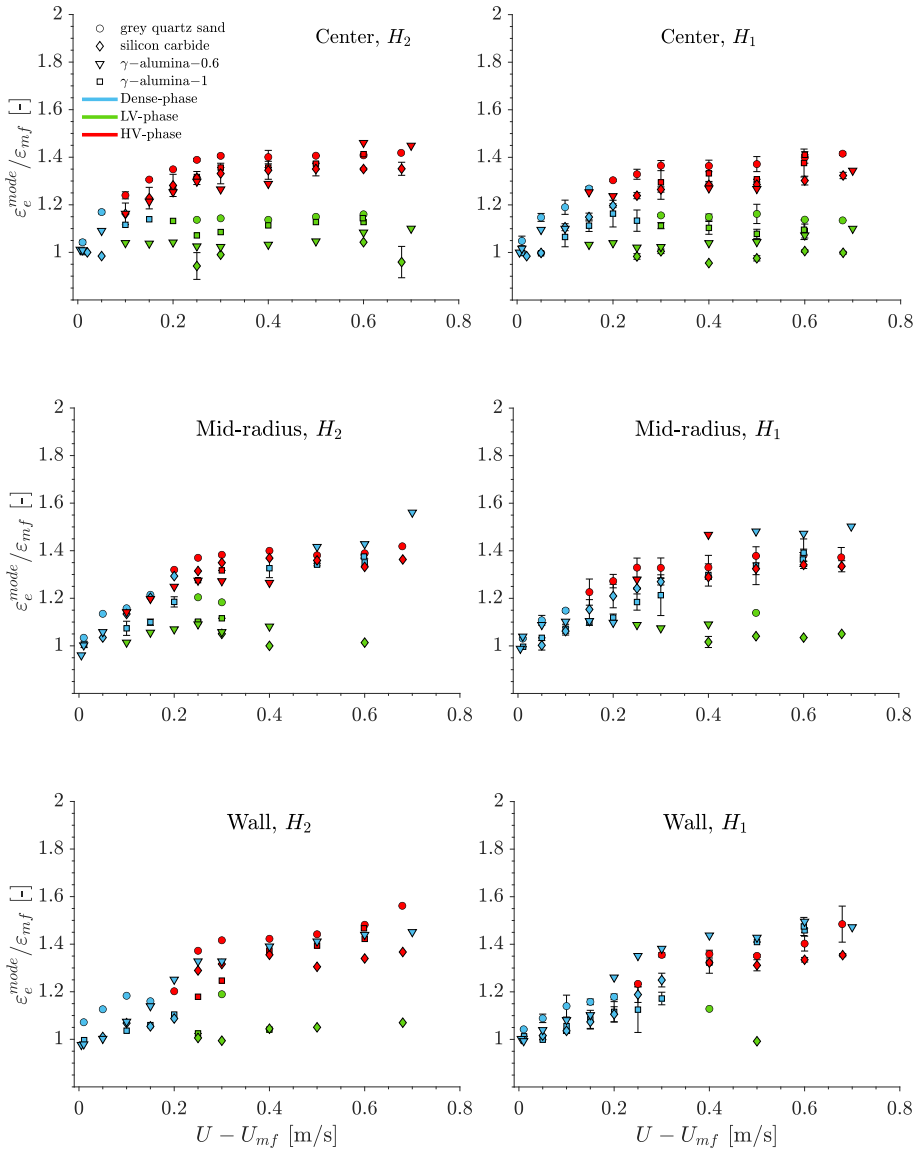

Fig. 14. Normalized mode values of the PDFs of the emulsion-phase voidage for the four material samples, at 500 °C, as a function of $U - U_{mf}$.

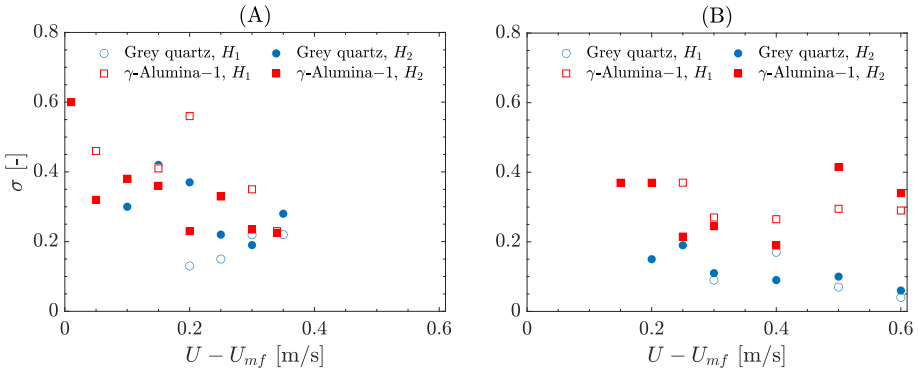

Fig. 15. The local LV-phase fraction in the emulsion phase at column axis for the grey quartz sand and γ-alumina–1 samples as function of $U - U_{mf}$. (A) Ambient temperature; (B) 500 °C.

Overall, results on voidage spatial distribution in bubbling fluidized beds of the four tested materials confirm that fluidization patterns of dense gas fluidized beds may largely depart from the two-phase theory as regards the voidage in the emulsion phase. Accordingly, the splitting of fluidizing gas between the bubble and the emulsion phase, and associated bubble flow patterns, must be investigated and correctly modelled.

Finally, the time series of the local voidage measured inside the bed

have been worked out to obtain the major features of the bubble phase, specifically the visible bubble flow. U_b has been determined by cross-correlating capacitance probe signals at H_1 and H_2 along bed axis; the bubble hold-up, δ, has been calculated from Eq. 9. Experimental estimation of bubble velocity by the signals cross-correlation method has been validated by measuring several bubbles velocity directly from signals observation in few chosen experimental conditions. Results are consistent with those from cross-correlations within a 6%. The visible bubble flow, determined at ambient temperature and 500 °C for the four tested materials, is reported in Fig. 16 as a function of the excess gas velocity with respect to minimum fluidization condition. The visible bubble flow does not significantly depend on the operating temperature but mainly on the excess of superficial gas velocity. At each value of $U - U_{mf}$, the visible bubble flow changes with bed material and increases according to the following order: silicon carbide, γ-alumina–1, grey quartz sand and γ-alumina–0.6. The experimental values of the visible bubble flow have been compared with predictions from the correlation of Fu et al. [57] (Fig. 17) valid for Geldart B and D solids. Overall, a fair agreement between experimental values and predictions is shown.

In the bed of grey quartz sand fluidized at ambient temperature and at $U - U_{mf} = 0.2$ m/s the mean measured bubble pierced length at H_2 is about 0.057 ± 0.02 m.

3.4. Estimate of emulsion-phase velocity

Figs. 18–19 report mean superficial gas velocities in the emulsion phase calculated with three different procedures (see paragraph 2.4) and normalized with respect to the minimum fluidization velocity of the samples at the temperature of interest as a function of $U - U_{mf}$ at ambient temperature and at 500 °C, respectively. The calculation of U_e from the correlation of Hilligardt and Werther [34] exclusively needs the value of minimum fluidization velocity of the considered bed material. U_e derived from the Richardson-Zaki correlation [35], instead, also depends on the measured mean emulsion-phase voidage averaged over bed section and the axial coordinate H_2 is used as reference. The calculation of U_e resulting from gas balance at the column cross section and at bed level H_2 is based on all variables measured by capacitance probe signals except the throughflow coefficient, which has been considered equal to 0, 1 and 3.

Analysis of Figs. 18–19 highlights that:

1) the values obtained from Eq. 3 of Hilligardt and Werther linearly depend on $U - U_{mf}$ and are nearby to those achieved by the third method based on gas balance with throughflow coefficients around/ slightly higher than unity [14], whatever bed temperature is considered;
2) the values calculated by the Eq. 4 (Richardson-Zaki correlation) increase linearly or slightly less than linearly with $U - U_{mf}$ whatever the bed temperature is considered. Some differences with bed temperature are observed if these values are compared with those obtained by the gas balance. At room temperature, U_e calculated with the Richardson-Zaki correlation is comparable with that calculated from gas balance with throughflow coefficients in the range 0–1 for the irregular bed materials (grey quartz sand and silicon carbide), instead a $k_{tf} \leq 0$ ("negative" throughflow coefficients) seems to represent data for γ-alumina fluidized particles. This discrepancy could be due to a non-negligible overestimation of the experimental visible bubble flow (see paragraph 3.3). For instance, experimental points associated to results on γ-alumina–0.6 at room temperature in Fig. 17 are those that mostly deviate upward from the bisect. Alternatively, this could simply suggest that the use of Richardson-Zaki correlation for U_e calculation for materials like the γ-alumina particles at ambient conditions, at least, can give misleading results. At 500 °C, U_e calculated with the Richardson-Zaki correlation is comparable with that calculated with gas balance with a throughflow coefficients in the range 0–1, but close to 1 for all the investigated bed materials;
3) the values calculated by the Eq. 2 (gas balance) increase linearly or slightly more than linearly with $U - U_{mf}$ whatever the bed temperature is considered and for the all the investigated bed materials. U_e/U_{mf} vs $U - U_{mf}$ curves parametric with the throughflow coefficient k_{tf} show that, obviously, the superficial gas velocity in the emulsion phase strongly increases with decreasing values of k_{tf} whatever bed temperature and bed material are considered;
4) the ratio of U_e/U_{mf}, evaluated at the same $U - U_{mf}$, is fairly constant with increasing temperature for all the bed materials. As a consequence, U_e, for instance, calculated according to Eq. 4 (Richardson-Zaki correlation) is systematically lower at 500 °C with respect to results at ambient temperature at the same $U - U_{mf}$;
5) from the comparison of the three methods applied to the four bed material samples at ambient temperature and 500 °C, it can be speculated that the throughflow coefficient can vary according to the operating conditions of the dense fluidized bed, namely operating temperature, superficial gas velocity, and bed material. This is in accordance with the results of Olowson and Almsted [16], who found no constant ratio between the bubble throughflow velocity, U_{tf}, and

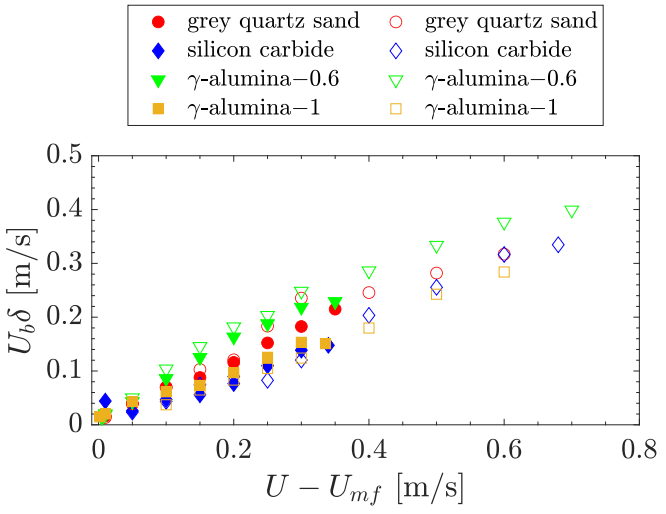

Fig. 16. Experimental visible bubble flow as a function of $U - U_{mf}$. Full symbols: ambient temperature; hollow symbols: 500 °C.

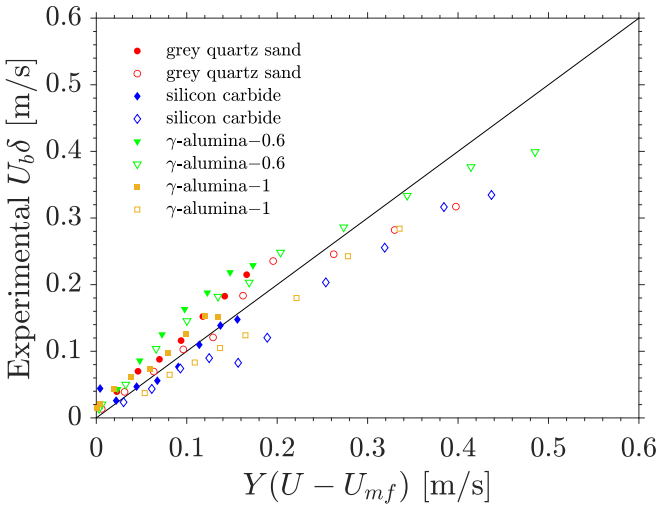

Fig. 17. Comparison between the measured visible bubble flow and the one predicted from the correlation of Fu et al. [57] valid for Geldart B and D solids and reported on the x-axis. Full symbols: ambient temperature; hollow symbols: 500 °C. $Y = 1.72Ar^{-0.133}(U - U_{mf})^{0.024}$.

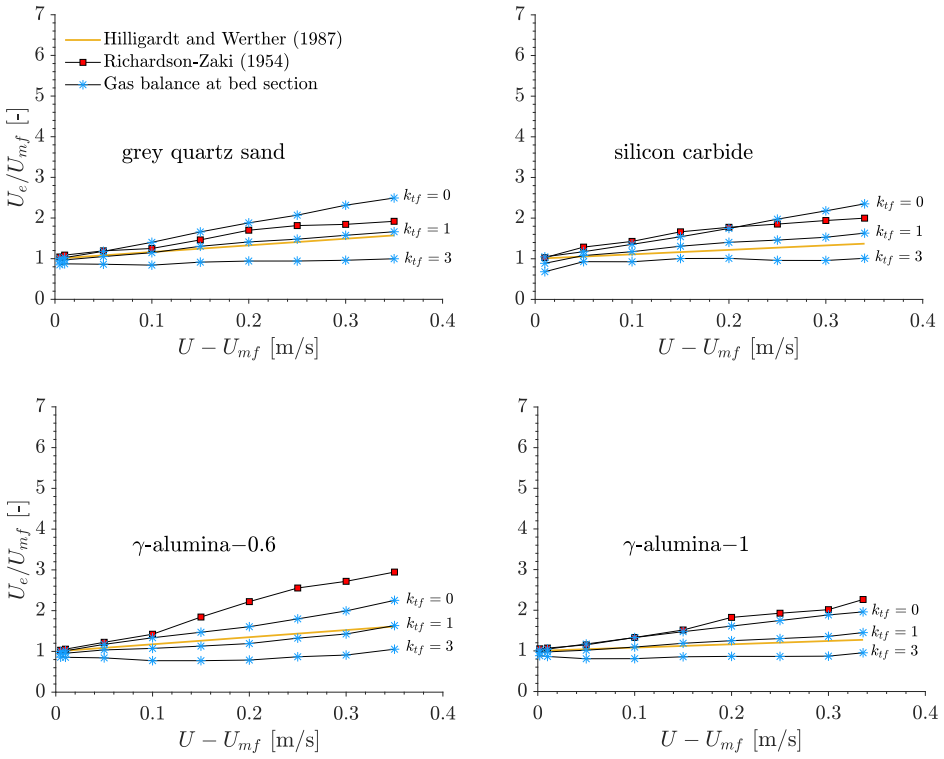

Fig. 18. Comparison of dimensionless emulsion-phase gas superficial velocities reported versus $U - U_{mf}$, obtained with the three different procedures reported in the paragraph 2.4, for the four bed materials. Room temperature.

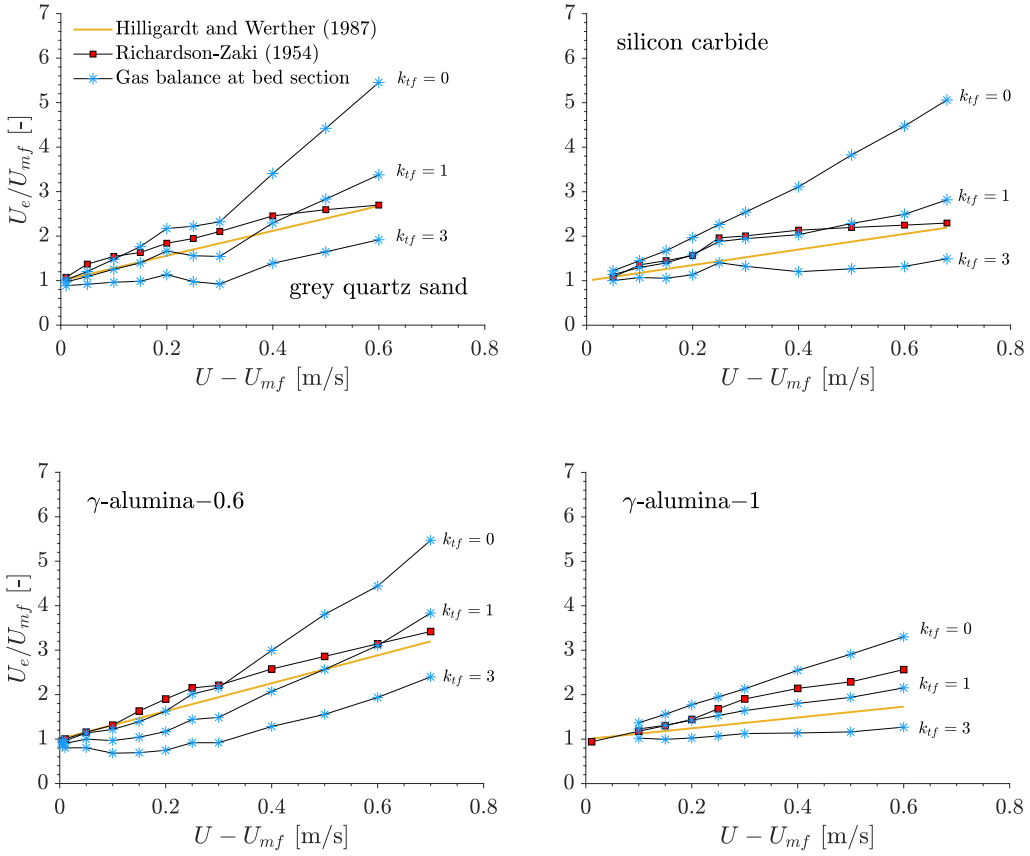

Fig. 19. Comparison of dimensionless emulsion-phase gas superficial velocities reported versus $U - U_{mf}$, obtained with the three different procedures reported in the paragraph 2.4, for the four bed materials. $T = 500$ °C.

emulsion phase superficial gas velocity, U_e. This is one of very few studies on throughflow velocity relative to bubbles in 3D beds operated at gas superficial velocities higher than U_{mf}. With their experimental apparatus, they measured a rather constant throughflow velocity relative to bubbles over the bed cross-section. Values of U_{tf} were of the order of four to five times U_{mf}. In our experiments, the same ratio U_{tf}/U_{mf} is rarely reached and only at high temperature. Results from Glicksman and McAndrews [15] cannot be considered for reliable comparisons because they refer to shallow 3D beds and do not consider the expansion of the emulsion phase as superficial gas velocity is increased in the gas balance of Eq. 1. In some cases, the comparison between the methods reported in Figs. 18–19 suggests an increase of k_{tf} with increasing excess gas velocity. This could be due to bubbles vertical coalescence, which typically enhances the throughflow component [11].

6) The influence of the particle size is also observed if the results of the two γ-alumina particles are compared. In particular, U_e/U_{mf} decreases as the particle size increases, especially for data obtained at 500 °C.
7) The data obtained from the three methods at 500 °C roughly collapse when the throughflow coefficient, k_{tf}, equal to 1 is considered for the method based on gas balance, whatever $U - U_{mf}$ and bed material are considered.

Overall, the analysis of the results highlights that:

- both the correlations proposed by Hilligart and Werther and by Richardson-Zaki can be reasonably used for the estimation of the emulsion phase velocity of Geldart B and D solids.
- The validity of the Richardson-Zaki correlation confirms that also for aggregative fluidization systems the emulsion phase can be treated as a homogeneous fluidized bed. This result is found to be perfectly in line with the study of Olowson and Almstedt [41] on bubbling fluidized beds of Geldart B/D solids. As a result, the expansion of the dense phase and the increase of U_e with respect to minimum fluidization condition act to keep the particle drag force equal to that at incipient fluidization condition.
- For the closure of the mass balance on the fluidized bed gas (Eq. 2), a throughflow coefficient, k_{tf} of the order of 1 can be used. Thus, $U_{tf} \cong U_e$ and the visible bubble flow is equal to $U - U_e$. This supports the fact that the two-phase theory overestimates the visible bubble flow since it does not consider the expansion of the emulsion phase and the consequent increase of the emulsion phase superficial velocity from U_{mf} to U_e.

3.5. Influence of emulsion phase characteristics on transport phenomena

Molignano et al. [42] demonstrated, performing mass transfer-limited reaction experiments, that the actual superficial gas velocity and voidage of the emulsion phase are needed to correctly predict Sherwood number around freely moving large active particles in bubbling fluidized beds. The authors carried out the catalytic oxidation of carbon monoxide at 450 °C over Pt-loaded γ-alumina spheres in the fluidized bed of grey quartz sand (Table 1). The experimental apparatus was the one represented in Fig. 1. The mass transfer coefficient around the freely moving active particles was measured from reaction conversion and worked out to calculate the particle Sherwood number, *Sh*. Experimental results were compared with those predicted by the proposed correlation (Eq. 6), in which the emulsion-phase superficial gas velocity in the Reynolds number of the active particle was calculated from Eq. 3 (Hilligardt and Werther [34] correlation). Consequently, the fitting parameter, *K*, turned out to be 0.84. Given the major relevance of the convective contribution over the diffusive one in Sherwood number [42], accurate determination of U_e is of fundamental importance. In Fig. 20, results from the study of Molignano et al. [42] on *Sh* versus $U -$

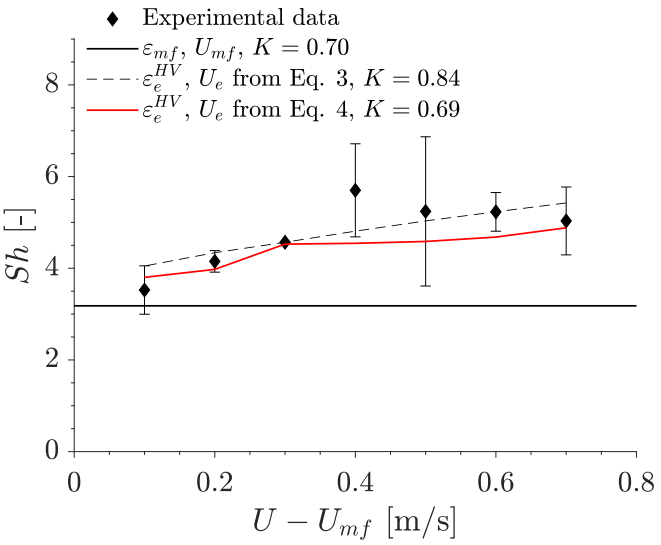

Fig. 20. Sherwood number as a function of excess gas superficial velocity. Data points at $T = 450$ °C and using grey quartz sand as bed material. Frössling-type correlations: black continuous line, $K = 0.70$, $U_e = U_{mf}$, $\varepsilon_e = \varepsilon_{mf}$ [64]; black dashed line, $K = 0.84$, U_e obtained from Eq. 3, $\varepsilon_e = \varepsilon_{HV}^{mode}$ [42]; red continuous line, $K = 0.69$ not used as fitting parameter, U_e obtained from Eq. 4 for the HV-phase, $\varepsilon_e = \varepsilon_{HV}^{mode}$. (For interpretation of the references to colour in this figure legend, the reader is referred to the web version of this article.)

U_{mf} are reported and compared with results from the present study. The red curve is obtained from Eq. 6, in which U_e values are calculated using the Richardson-Zaki correlation (Eq. 4) with ε_{HV}^{mode} (averaged over the column cross section at H_2) as representative emulsion-phase voidage value. The outcomes are remarkable: the red curve is obtained from Eq. 6 in which *K* is not a fitting parameter. *K* is set equal to 0.69, a consolidated number in literature as it derives from the study of Rowe et al. [62], who extended the results on mass transfer around isolated particles by Ranz and Marshall [63] to Reynolds numbers comprised between 20 and 2000.

In conclusion, the hydrodynamics of the investigated bubbling fluidized beds do have an impact on mass transfer. Accordingly, consequences on heat transfer coefficients are also expected for fluidized beds exhibiting such peculiar bed voidage distribution. The assumption of the two-phase theory may lead to incorrect modeling of heat transfer as well. This aspect has been addressed in the studies of Stefanova et al. [65,66], in which voidage distribution of fluidized beds near the transition to the turbulent fluidization flow regime and in the turbulent regime has been characterized. The presence of structures of intermediate voidage between dense phase at minimum fluidization conditions and a more diluted phase, typically known as voids, is observed. In this context, taking into account the contributions of such structures of intermediate voidage is mandatory for the correct predictions of heat transfer coefficients.

4. Conclusions

The hydrodynamics of dense fluidized beds of different solids belonging to groups B and D of Geldart's classification, operated at ambient temperature and 500 °C, have been successfully characterized using capacitance probes.

Statistical analysis of the time-series of local bed voidage yields probability density functions parametric in the excess gas velocity, $U - U_{mf}$. The bimodal character in the portion of the spectrum that refers to the emulsion phase of the bed, more pronounced as the gas superficial velocity is increased, is present in all the tested materials at specific experimental conditions. The comparison between the different mate-

rials confirms that the higher-voidage phase (HV) can be mainly attributed to bed dilatancy associated with bubble-induced shear flow. Instead, the hypothesis that it reflects the presence of the bubble cloud is more unlikely.

With reference to the composite nature of the emulsion phase in the dense gas fluidized bed of monodisperse solids, irregular solids and spherical particles present some different peculiar features, as revealed from the statistical approach. This aspect demonstrates that surface properties could significantly influence emulsion phase expansion as the result of bubble-induced shear flow. In spite of the highlighted differences, the characteristic voidages associated with the emulsion phase of the four tested materials show similar trends with superficial gas velocity excess with respect to minimum fluidization conditions. This aspect has been demonstrated by the representation of data normalized with respect to the voidage values at incipient fluidization. Although results obtained at 500 °C qualitatively resemble those obtained at ambient temperature, quantitative differences are observed, confirming the need for characterization of bed hydrodynamics at temperatures of interest in industrial applications.

Results on bed voidage distribution by capacitance probes, especially with reference to the detected emulsion phase expansion, stimulated the investigation of the associated deviation of superficial gas velocity from that at minimum fluidization condition. The Richardson-Zaki correlation, in which the measured emulsion phase voidage is implemented, predicts superficial gas velocity values associated to the emulsion-phase which fall in a reasonable range, as also confirmed by comparison with results from gas balance at the bed cross-section and from Hilligardt and Werther [34] correlation. The proper features of the emulsion phase in terms of superficial gas velocity and voidage are crucial to correctly predict the Sherwood number for gas mass transfer between the bulk of the bed and freely-moving large active particles. It was demonstrated that the utilization of the measured expanded emulsion-phase voidage along with the associated values of superficial gas velocity calculated by the Richardson-Zaki correlation allows to correctly estimate Sherwood numbers obtained in a previous experimental study using a Frössling-type equation without fitting parameters. This result further confirms, with a reasonable level of approximation, the validity of the Richardson-Zaki correlation also in the field of aggregative fluidization. This subject also finds confirmation in some relevant literature studies [37,39], in which experimental evidence is supported by a theoretical approach [41].

Overall, results on hydrodynamic characterization of monodisperse fluidized beds find some confirmation in the literature and provide new insights about fundamentals of fluidization. Although results have been obtained on a relatively small unit, the proposed approach to the investigated phenomena constitutes a good starting point for phenomenological studies at larger scale units.

CRediT authorship contribution statement

Laura Molignano: Writing – original draft, Visualization, Validation, Software, Methodology, Investigation, Formal analysis, Conceptualization. **Maurizio Troiano:** Writing – review & editing, Supervision, Conceptualization. **Roberto Solimene:** Writing – review & editing, Supervision, Resources, Project administration, Funding acquisition, Conceptualization. **Sina Tebianian:** Writing – review & editing, Supervision. **Jean-Francois Joly:** Funding acquisition. **Piero Salatino:** Writing – review & editing, Funding acquisition, Conceptualization.

Declaration of competing interest

The authors declare that they have no known competing financial interests or personal relationships that could have appeared to influence the work reported in this paper.

Data availability

Data will be made available on request.

Acknowledgements

The authors gratefully acknowledge Mr. Antonio Cammarota for the set-up of the experimental apparatus, and Mr. Christian Tracol and Mr. Vincent Bracco for the SEM analyses of the samples. Authors wish also to express their gratitude to Ms. Cristiana Rocca and Mr. Mario Mobiglia, University of Naples, for the support during the experimental campaign.

Appendix A. Supplementary data

Supplementary data to this article can be found online at https://doi.org/10.1016/j.powtec.2024.120174.

References

[1] J.R. Grace, Chapter 1: Introduction, history, and applications, in: J. Grace, X. Bi, N. Ellis (Eds.), Essentials of Fluidization Technology, First Edition, Wiley-VCH, 2020, pp. 1–9, https://doi.org/10.1002/9783527699483.ch1.
[2] R. Toomey, H.F. Johnstone, Gas fluidization of solid particles, Chem. Eng. Prog. 48 (1952) 220–226.
[3] J.R. Grace, R. Clift, On the two-phase theory of fluidization, Chem. Eng. Sci. 29 (1974) 327–334, https://doi.org/10.1016/0009-2509(74)80039-4.
[4] D.L. Pyle, D. Harrison, An experimental investigation of the two-phase theory of fluidization, Chem. Eng. Sci. 22 (1967) 1199–1207, https://doi.org/10.1016/0009-2509(67)80186-6.
[5] P.N. Rowe, L. Santoro, J.G. Yates, The division of gas between bubble and interstitial phases in fluidised beds of fine powders, Chem. Eng. Sci. 33 (1978) 133–140, https://doi.org/10.1016/0009-2509(78)85079-9.
[6] I.A. Khattab, C. Kuroda, M. Ishida, Radial and vertical distributions of the interstitial gas velocity in a fluidized bed, J. Chem. Eng. Japan. 21 (1988) 282–287, https://doi.org/10.1252/jcej.21.282.
[7] H. Cui, N. Mostoufi, J. Chaouki, Characterization of dynamic gas-solid distribution in fluidized beds, Chem. Eng. J. 79 (2000) 133–143, https://doi.org/10.1016/S1385-8947(00)00178-9.
[8] H. Cui, N. Mostoufi, J. Chaouki, Gas and solids between dynamic bubble and emulsion in gas-fluidized beds, Powder Technol. 120 (2001) 12–20, https://doi.org/10.1016/S0032-5910(01)00341-2.
[9] M.J. Lockett, J.F. Davidson, D. Harrison, On the two-phase theory of fluidization, Chem. Eng. Sci. 22 (1967) 1059–1066, https://doi.org/10.1016/0009-2509(67)80170-2.
[10] J.R. Grace, D. Harrison, The behaviour of freely bubbling fluidised beds, Chem. Eng. Sci. 24 (1969) 497–508, https://doi.org/10.1016/0009-2509(69)85021-9.
[11] J.A. Valenzuela, L.R. Glicksman, Gas flow distribution in a bubbling fluidized bed, Powder Technol. 44 (1985) 103–113, https://doi.org/10.1016/0032-5910(85)87016-9.
[12] J.F. Davidson, D. Harrison, The behaviour of a continuously bubbling fluidised bed, Chem. Eng. Sci. 21 (1966) 731–738, https://doi.org/10.1016/0009-2509(66)87001-X.
[13] J.F. Davidson, D. Harrison, Fluidised Particles, First Edition, Cabridge Press, New York, 1963, https://doi.org/10.1002/aic.690100503.
[14] J.D. Murray, On the mathematics of fluidization part 2. Steady motion of fully developed bubbles, J. Fluid Mech. 22 (1965) 57–80, https://doi.org/10.1017/S0022112065000587.
[15] L.R. Glicksman, G. McAndrews, The effect of bed width on the hydrodynamics of large particle fluidized beds, Powder Technol. 42 (1985) 159–167, https://doi.org/10.1016/0032-5910(85)80049-8.
[16] P.A. Olowson, A.E. Almstedt, Influence of pressure and fluidization velocity on the bubble behaviour and gas flow distribution in a fluidized bed, Chem. Eng. Sci. 45 (1990) 1733–1741, https://doi.org/10.1016/0009-2509(90)87051-S.
[17] L. Hailu, F. Plaka, R. Clift, J.F. Davidson, Measurement of gas flow through a two-dimensional bubble in a fluidised bed, Chem. Eng. Res. Des. 71 (1993) 382–389.
[18] M. Gautam, J.T. Jurewicz, S.R. Kale, An experimental investigation of throughflow velocities in two-dimensional fluidized bed bubbles: laser doppler anemometer measurements, J. Fluids Eng. Trans. ASME. 116 (1994) 605–612, https://doi.org/10.1115/1.2910320.
[19] K.S. Lim, V.S. Gururajan, P.K. Agarwal, Mixing of homogeneous solids in bubbling fluidized beds: theoretical modelling and experimental investigation using digital image analysis, Chem. Eng. Sci. 48 (1993) 2251–2265, https://doi.org/10.1016/0009-2509(93)80241-H.
[20] W. Wu, P.K. Agarwal, The effect of bed temperature on mass transfer between the bubble and emulsion phases in a fluidized bed, Can. J. Chem. Eng. 81 (2003) 940–948, https://doi.org/10.1002/cjce.5450810503.
[21] S.P. Sit, J.R. Grace, Effect of bubble interaction on interphase mass transfer in gas fluidized beds, Chem. Eng. Sci. 36 (1981) 327–335, https://doi.org/10.1016/0009-2509(81)85012-9.

[22] R. Solimene, A. Marzocchella, G. Passarelli, P. Salatino, Assessment of gas-fluidized beds mixing and hydrodynamics by zirconia sensors, AICHE J. 52 (2006) 185–198, https://doi.org/10.1002/aic.10592.
[23] J.A. Almendros-Ibáñez, D. Pallarès, F. Johnsson, D. Santana, Voidage distribution around bubbles in a fluidized bed: influence on throughflow, Powder Technol. 197 (2010) 73–82, https://doi.org/10.1016/j.powtec.2009.08.021.
[24] A. Bakshi, A.F. Ghoniem, C. Altantzis, Mixing dynamics in bubbling fluidized beds, AICHE J. 63 (2017) 4316–4328, https://doi.org/10.1002/aic.15801.
[25] J.G. Villanueva-Chávez, W.A. Bizzo, Fluid dynamic modeling of a large bubbling fluidized bed for biomass combustion: mass transfer in bubbles, Chem. Eng. Sci. 196 (2019) 414–424, https://doi.org/10.1016/j.ces.2018.11.023.
[26] L. Shen, F. Johnsson, B. Leckner, Digital image analysis of hydrodynamics two-dimensional bubbling fluidized beds, Chem. Eng. Sci. 59 (2004) 2607–2617, https://doi.org/10.1016/j.ces.2004.01.063.
[27] A. Vepsäläinen, S. Shah, J. Ritvanen, T. Hyppänen, Interphase mass transfer coefficient in fluidized bed combustion by Eulerian CFD modeling, Chem. Eng. Sci. 106 (2014) 30–38, https://doi.org/10.1016/j.ces.2013.11.042.
[28] P. Salatino, R. Solimene, Mixing and segregation in fluidized bed thermochemical conversion of biomass, Powder Technol. (2017), https://doi.org/10.1016/j.powtec.2016.11.058.
[29] T. Li, H. Thunman, H. Ström, A fast-solving particle model for thermochemical conversion of biomass, Combust. Flame 213 (2020) 117–131, https://doi.org/10.1016/j.combustflame.2019.11.018.
[30] M. Troiano, A. Cammarota, C. Tregambi, R. Chirone, P. Salatino, R. Solimene, Fluidized bed combustion of solid lignin-rich residues from bioethanol production, Powder Technol. 371 (2020) 170–179, https://doi.org/10.1016/j.powtec.2020.05.070.
[31] K.Y. Kwong, R. Mao, S.A. Scott, J.S. Dennis, E.J. Marek, Analysis of the rate of combustion of biomass char in a fluidised bed of CLOU particles, Chem. Eng. J. 417 (2021) 127942, https://doi.org/10.1016/j.cej.2020.127942.
[32] A.N. Hayhurst, M.S. Parmar, Measurement of the mass transfer coefficient and Sherwood number for carbon spheres burning in a bubbling fluidized bed, Combust. Flame 130 (2002) 361–375, https://doi.org/10.1016/S0010-2180(02)00387-5.
[33] F. Scala, A new technique for the measurement of the product CO/CO_2 ratio at the surface of char particles burning in a fluidized bed, Proc. Combust. Inst. 32 II (2009) 2021–2027, https://doi.org/10.1016/j.proci.2008.06.047.
[34] K. Hilligardt, J. Werther, Influence of temperature and properties of solids on the size and growth of bubbles in gas fluidized beds, Chem. Eng. Technol. 10 (1987) 272–280, https://doi.org/10.1002/ceat.270100133.
[35] J.F. Richardson, W.N. Zaki, Sedimentation and fluidisation. Part 1, Trans. Inst. Chem. Eng. 32 (1954) 35–53.
[36] A.R. Khan, J.F. Richardson, Fluid-particle interactions and flow characteristics of fluidized beds and settling suspensions of spherical particles, Chem. Eng. Commun. 78 (1989) 111–130, https://doi.org/10.1080/00986448908940189.
[37] R. Di Felice, Hydrodynamics of liquid fluidisation, Chem. Eng. Sci. 50 (1995) 1213–1245, https://doi.org/10.1016/0009-2509(95)98838-6.
[38] P. Lettieri, D. Newton, J.G. Yates, Homogeneous bed expansion of FCC catalysts, influence of temperature on the parameters of the Richardson-Zaki equation, Powder Technol. 123 (2002) 221–231, https://doi.org/10.1016/S0032-5910(01)00463-6.
[39] L.G. Gibilaro, Chapter 4: Homogeneous fluidization, in: L.G. Gibilaro (Ed.), Fluidization Dynamics, First Edition, Butterworth-Heinemann, 2001, pp. 31–41, https://doi.org/10.1016/B978-075065003-8/50007-0.
[40] A.A. Avidan, J. Yerushalmi, Bed expansion in high velocity fluidization, Powder Technol. 32 (1982) 223–232, https://doi.org/10.1016/0032-5910(82)85024-9.
[41] P.A. Olowson, A.E. Almstedt, Hydrodynamics of a bubbling fluidized bed: influence of pressure and fluidization velocity in terms of drag force, Chem. Eng. Sci. 47 (1992) 357–366, https://doi.org/10.1016/0009-2509(92)80026-9.
[42] L. Molignano, M. Troiano, R. Solimene, S. Tebianian, F. Scala, P. Salatino, J.F. Joly, Hydrodynamics and mass transfer around active particles in dense gas-fluidized beds, Fuel 341 (2023) 127590, https://doi.org/10.1016/j.fuel.2023.127590.
[43] N. Frössling, On the evaporation of falling drops, Gerlands Beitrage Zur Geophys. 52 (1938) 170.
[44] R.D. La Nauze, K. Jung, The kinetics of combustion of petroleum coke particles in a fluidized-bed combustor, in: Proc. Combust. Inst, 1982, pp. 1087–1092, https://doi.org/10.1016/S0082-0784(82)80284-1.
[45] J. Werther, O. Molerus, The local structure of gas fluidized beds - I. A statistically based measuring system, Int. J. Multiphase Flow 1 (1973) 103–122, https://doi.org/10.1016/0301-9322(73)90007-4.
[46] A. Lancia, R. Nigro, G. Volpicelli, L. Santoro, Transition from slugging to turbulent flow regimes in fluidized beds detected by means of capacitance probes, Powder Technol. 56 (1988) 49–56, https://doi.org/10.1016/0032-5910(88)80021-4.
[47] A. Lancia, R. Nigro, L. Santoro, G. Volpicelli, Characterization of the quality of slugging regime in fluidized beds by means of two capacitance probes, Adv. Powder Technol. 2 (1991) 37–47, https://doi.org/10.1016/S0921-8831(08)60719-0.
[48] V. Wiesendorf, J. Werther, Capacitance probes for solids volume concentration and velocity measurements in industrial fluidized bed reactors, 2000, https://doi.org/10.1016/S0032-5910(99)00276-4.
[49] T. Wytrwat, M. Yazdanpanah, S. Heinrich, Bubble properties in bubbling and turbulent fluidized beds for particles of Geldart's group B, Processes 8 (2020), https://doi.org/10.3390/pr8091098.
[50] J.R. Grace, Chapter 2: Properties, minimum fluidization, and Geldart groups, in: J. Grace, X. Bi, N. Ellis (Eds.), Essentials of Fluidization Technology, First Edition, Wiley-VCH, 2020, pp. 11–32, https://doi.org/10.1002/9783527699483.ch2.
[51] W.-C. Yang, Chapter 2: Flow through fixed beds, in: W.-C. Yang (Ed.), Handbook of Fluidization and Fluid-Particle Systems, First edition, CRC Press, 2003, pp. 29–52, https://doi.org/10.1016/s1672-2515(07)60126-2.
[52] D. Kunii, O. Levenspiel, Chapter 3: Fluidization and mapping of regimes, in: D. Kunii, O. Levenspiel (Eds.), Fluidization Engineering, Second Edition, Butterworth-Heinemann, 1991, pp. 61–94, https://doi.org/10.1016/b978-0-08-050664-7.50009-3.
[53] T.M. Knowlton, Pressure and temperature effects in fluid-particle systems, in: O. E. Potter, D.J. Nicklin (Eds.), Fluid. 7, Engineering Foundation, New York, 1992, pp. 27–46, https://doi.org/10.1016/B978-081551427-5.50004-1.
[54] B. Formisani, R. Girimonte, L. Mancuso, Analysis of the Fluidization Process of Particle Beds at High Temperature, 1998, https://doi.org/10.1016/S0009-2509(97)00370-9.
[55] D. Falkowski, R.C. Brown, Analysis of pressure fluctuations in fluidized beds, Ind. Eng. Chem. Res. 43 (2004) 5721–5729, https://doi.org/10.1021/ie030684u.
[56] H.T. Bi, N. Ellis, I.A. Abba, J.R. Grace, A state-of-the-art review of gas–solid turbulent fluidization, Chem. Eng. Sci. 55 (2000) 4789–4825, https://doi.org/10.1016/S0009-2509(00)00107-X.
[57] Z. Fu, J. Zhu, S. Barghi, Y. Zhao, Z. Luo, C. Duan, On the two-phase theory of fluidization for Geldart B and D particles, Powder Technol. 354 (2019) 64–70, https://doi.org/10.1016/j.powtec.2019.05.051.
[58] R. Andreux, J. Chaouki, Behaviors of the bubble, cloud, and emulsion phases in a fluidized bed, AICHE J. 54 (2008) 406–414, https://doi.org/10.1002/aic.11390.
[59] Y. Forterre, O. Pouliquen, Flows of dense granular media, Annu. Rev. Fluid Mech. 40 (2008) 1–24, https://doi.org/10.1146/annurev.fluid.40.111406.102142.
[60] H.T. Bi, Local phase holdups in gas-solids fluidization and transport, AICHE J. 47 (2001) 2025–2031, https://doi.org/10.1002/aic.690470913.
[61] D. Kunii, O. Levenspiel, Chapter 5: Bubbles in dense beds, in: D. Kunii, O. Levenspiel (Eds.), Fluidization Engineering, Second Edition, Butterworth-Heinemann, 1991, pp. 115–135, https://doi.org/10.1016/b978-0-08-050664-7.50011-1.
[62] P.N. Rowe, K.T. Claxton, J.B. Lewis, Heat and mass transfer from a single sphere in an extensive flowing fluid, Trans. Inst. Chem. Eng. 43 (1965) 14–31.
[63] W.E. Ranz, W.R. Marshall Jr., Evaporation from drops, Chem. Eng. Prog. 48 (1952), 141–146 and 173–180.
[64] F. Scala, Mass transfer around freely moving active particles in the dense phase of a gas fluidized bed of inert particles, Chem. Eng. Sci. 62 (2007) 4159–4176, https://doi.org/10.1016/j.ces.2007.04.040.
[65] A. Stefanova, H.T. Bi, C.J. Lim, J.R. Grace, Heat transfer from immersed vertical tube in a fluidized bed of group A particles near the transition to the turbulent fluidization flow regime, Int. J. Heat Mass Transf. 51 (2008) 2020–2028, https://doi.org/10.1016/j.ijheatmasstransfer.2007.06.005.
[66] A. Stefanova, X.T. Bi, C. Jim Lim, J.R. Grace, A probabilistic heat transfer model for turbulent fluidized beds, Powder Technol. 365 (2020) 163–171, https://doi.org/10.1016/j.powtec.2019.01.066.